Lithos 179 (2013) 67–83

Contents lists available at ScienceDirect

Lithos

journal homepage: www.elsevier.com/locate/lithos

Subduction controls on Miocene back-arc lavas from Sierra de Huantraico and La Matancilla and new $^{40}Ar/^{39}Ar$ dating from the Mendoza Region, Argentina

Charlotte T. Dyhr [a,*], Paul M. Holm [a], Eduardo J. Llambías [b], Anders Scherstén [c]

[a] Department of Geography and Geology, University of Copenhagen, Oster Voldgade 10, DK-1350 Copenhagen, Denmark
[b] Universidad Nacional de La Plata, Calle 1#644, La Plata, Argentina
[c] Department of Geology, Lund University, Sölvegatan 12, S-223 62 Lund, Sweden

ARTICLE INFO

Article history:
Received 4 January 2013
Accepted 5 August 2013
Available online 15 August 2013

Keywords:
Back-arc/arc transition
Flat slab subduction
$^{40}Ar/^{39}Ar$ dating

ABSTRACT

Back-arc volcanism in the western Argentinian provinces of Mendoza and Neuquén has been widespread from the Miocene to historic times. We present a detailed investigation of profiles through two of the major Miocene volcanic areas of the region, the neighboring Huantraico and La Matancilla plateaus, including new $^{40}Ar/^{39}Ar$ age results of major and trace elements as well as Nd, Sr and Pb isotopic data. Four million years of eruptions from 24.4 ± 0.3 Ma (2σ) of alkali olivine basalts with OIB-type incompatible trace element enrichments at La Matancilla (~36.50°S) provide evidence for the presence of back-arc mantle devoid of subduction-related components. In contrast, the lower Huantraico lavas (~37.30°S) require an atypical back-arc mantle, almost devoid of arc-like components (e.g. low La/Ta = 15–18 and Ba/La = 12–18), but with a more depleted isotopic signature (e.g. $^{87}Sr/^{86}Sr$, 0.7033–0.7037) than observed elsewhere in the Andean back-arc. The Lower to Upper Series development in the Huantraico sequence represents a gradual change from basaltic to trachyandesitic back-arc lavas with a weak but temporally increasing arc geochemical signature (e.g. La/Ta = 15–21; Ba/La = 12–45), which is accompanied by Sr, Nd and Pb isotopic compositions approaching present day values of the Andes arc. The compositional change is accompanied by a gradually decreasing role for garnet in the mantle source, a decreasing degree of melting, but also simultaneously increasing influence from subducted fluids, probably as the slab geometry changes through time. The volcanism at Huantraico ceased when a flat slab was established around 15 Ma.

1. Introduction

Early to mid-Miocene volcanic rocks were erupted in the Neuquén Basin after a change from slower, more oblique South America–Farallon plate convergence to more rapid, near-normal South America–Nazca plate convergence (ca. 25–24 Ma (Jordan et al., 2001; Kay and Copeland, 2006; Pardo-Casas and Molnar, 1987; Somoza, 1998)). The Miocene magmatic evolution in the back-arc can be divided into three stages. During stage 1 (24–20 Ma) back-arc alkali olivine basaltic lavas were erupted across the Neuquén Basin, e.g. in La Matancilla (~36°50′S) (Fig. 1). The second magmatic stage (20–18 Ma (Kay and Copeland, 2006)), which constitutes the main focus of this study, produced basalts to trachyandesites outcropping in the southern and central Sierra de Huantraico (37°S–37°40′S) (Fig. 1). We prolong the timing of this stage slightly to 17.5 Ma on the basis of new $^{40}Ar/^{39}Ar$ dating. Kay and Copeland (2006) suggest that the concentration of Pichi Tril andesites in the southeastern Sierra de Huantraico marks the principal eruptive center and the eruptive cycle is suggested to have started with an explosive event. During this stage, a subduction related component was introduced into the back-arc mantle beneath the Neuquén Basin (at ca. 20 Ma), possibly in association with the initiation of shallowing of the subducting Nazca plate (e.g. Kay, 2001; Kay et al, 2006). From 19 to 17 Ma basalts to andesites were erupted from volcanic complexes in the Sierra de Huantraico and Sierra Negro in Southern Mendoza (Cobbold and Rossello, 2003; Kay and Copeland, 2006; Kay et al., 2006; Nullo et al., 2002). We describe the lavas of Sierra de Huantraico and present new information on their geological age, petrography and geochemical characteristics. These magmas have a weak arc-like signature (La/Ta = 15–25, Ba/La = 12–20, Ta/Hf = 0.25–0.4), flatter REE patterns and less enriched isotope signatures than e.g. Chachahuén lavas (Kay et al., 2006). The arc signature increases with decreasing age. Kay and Copeland (2006) argue that these magmas were generated in a mantle containing subducted components in a contractional setting (Cobbold and Rossello, 2003; Viñes, 1990) and we shed new light on the nature of such subducted material in the back-arc mantle. During the third volcanic stage (16–15 Ma), the andesitic Cerro Bayo de Sierra Negro center was produced. Gonzáles Díaz (1979) also ascribes the

* Corresponding author. Tel.: +45 3532 2467.
E-mail addresses: ctd@geo.ku.dk (C.T. Dyhr), paulmh@geo.ku.dk (P.M. Holm), llambias@cig.museo.unlp.edu.ar (E.J. Llambías), Anders.Schersten@geol.lu.se (A. Scherstén).

0024-4937/$ – see front matter © 2013 Elsevier B.V. All rights reserved.
http://dx.doi.org/10.1016/j.lithos.2013.08.007

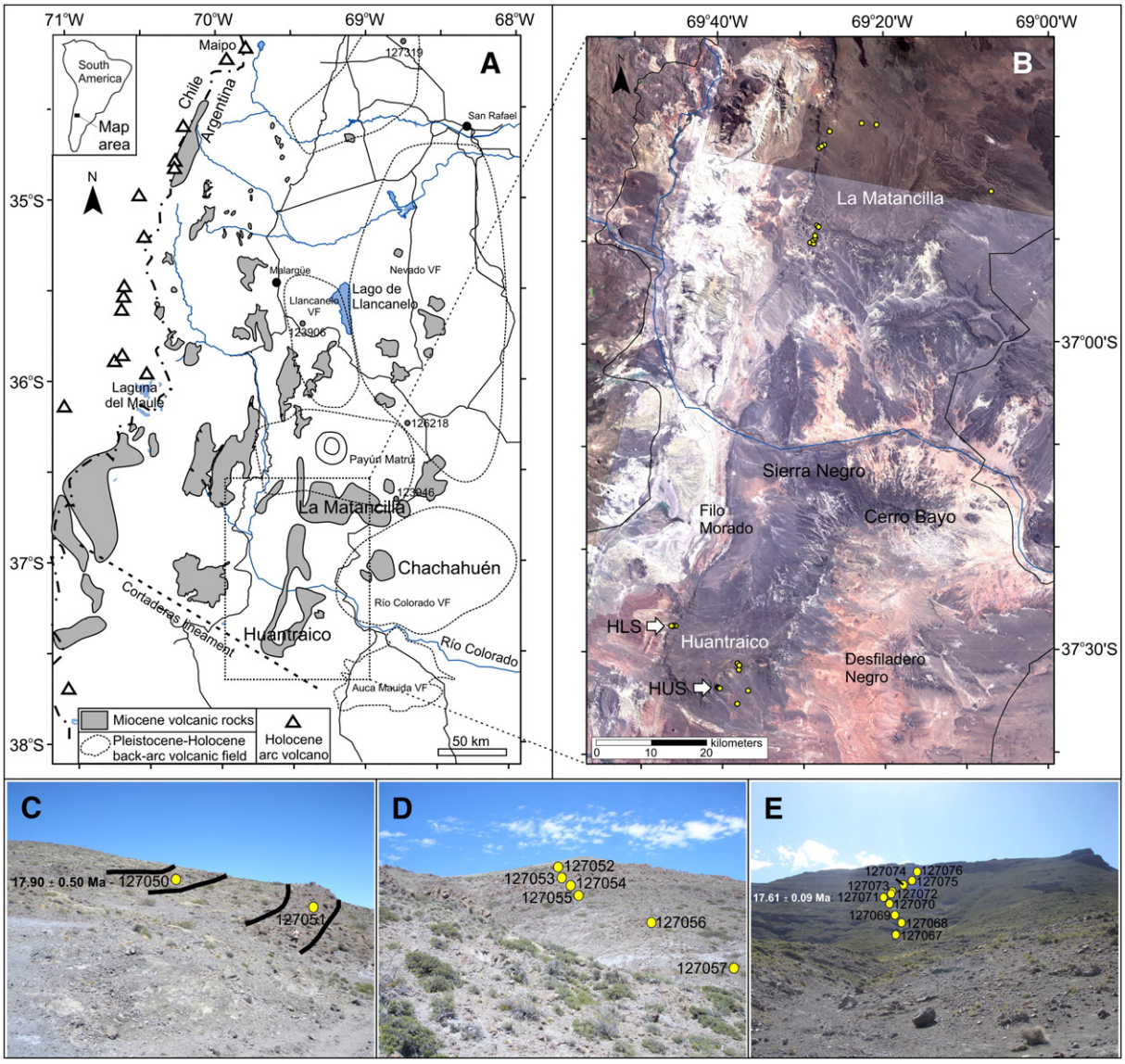

Fig. 1. A) Generalized map of volcanic areas of southern Mendoza and northern Neuquen based on Nullo et al. (2002), Ramos and Kay (2006), Kay and Copeland (2006), Litvak et al. (2008), Sruoga et al. (2008), Gudnasson et al. (2012), and Spagnuolo et al. (2012). Gray circles: Sample location for dated Pleistocene samples. B) Satellite photograph of La Matancilla and Huantraico areas. Yellow circles mark collected lava flows and dikes. HLS—Huantraico Lower Series profile, HUS—Huantraico Upper Series profile. C) Samples 127050 and 127051 are the uppermost of the Lower Huantraico. D) The bulk of Lower Huantraico lavas are samples in one profile. Samples 127058–127063, including dated sample 127062 (17.80 ± 0.20 Ma), belonging to lower Huantraico are not shown in lower panel photographs as they are below the area shown in C). E) Upper Huantraico series.

Cerro El Ramblón flow in the La Matancilla region to this eruption cycle. Existing ages are consistent with a gap in magmatism from ca. 17 to 16 Ma and a subsequent break in back-arc magmatism, east of 70.20°W, in northern Neuquén and southern Mendoza lasting until approximately 9 Ma. However, as noted by Kay et al. (2006) arc type magmatism occurs from 14 to 10 Ma in the Trappa Trappa Formation and Huincan. Post-Miocene alkaline flows are associated with the Llancanelo, Payún Matrú and Auca Mahuída volcanic fields that cover a vast part of the back-arc, north of the Cortaderas lineament (Fig. 1B).

Chemical contrasts between 24–20 Ma and 20–17 Ma (stage 1 and stage 2) flows are consistent with changes in the composition of the mantle source as the tectonic regime became contractional after 20 Ma (Kay and Copeland, 2006). These changes are explored by comparing the chemistry and isotopic compositions of Huantraico back-arc lavas to those of Miocene La Matancilla and Pliocene–Pleistocene Río Colorado intraplate magmas and recent arc magmas from Maipo and Laguna del Maule. The first Miocene magmatic cycle (24–20 Ma) is characterized by intraplate ocean island basalt (OIB) chemical signatures. Their mantle sources are nearly devoid of subduction-type components, which are shown by enriched high field strength element (HFSE) concentrations relative to the light rare earth elements (LREE) (indicated by La/Ta < 14), a lack of evidence for subducted crustal material (shown by Th/La = 0.09–0.13 (<0.12 in MORB–OIB lavas)) and a lack of evidence for excess fluid-mobile hydrous elements (Ba/La ratios, <16). The second magmatic episode reflects the transient entry of a subduction zone component into the back-arc mantle evidenced by e.g. La/Ta >15, higher Th/La ratios than OIB lavas (>0.15) and Ba/La ratios between 14 and 20.

To contribute to the understanding of the origin of continental back-arc basalts and the transition from back-arc to arc petrogenesis we present major and trace elements with Sr, Nd and Pb isotopic compositions of Miocene basalts from the Huantraico plateau. We also present 10 new $^{40}Ar/^{39}Ar$ radiometric ages from the Sierra de Huantraico and surrounding provinces and characterize the petrology of the Huantraico volcanic

rocks. Detailed sampling of stratigraphic sections allows us to further develop current hypotheses of the evolution of the asthenosphere–lithosphere system at this convergent margin. Evidence for increasing slab-influence, possibly in accordance with a small decrease in subduction rate and/or shallowing of the subduction angle of the Nazca plate comes from nepheline to hypersthene normative compositions (ne–hy content is well correlated to e.g. Ba/Nb ratios with high Ba/Nb rocks corresponding to hypersthene normative rocks), increasingly arc-like incompatible trace element ratios, increasing Sr and Pb isotopic ratios and decreasing Nd isotopic ratios.

2. Geological setting and previous chronological studies in the Huantraico region

The Miocene lavas that are the focus of this study occur from 69.30°W to 69.50°W and from 37.25°S to 37.35°S (Fig. 1). They overlie Mesozoic–early Tertiary sedimentary sequences that fill the northern and central parts of Neuquén Basin. The Cortaderas lineament lies along a NW-trending regional structure and projects into the modern Southern Volcanic Zone (Kay and Copeland, 2006). To the south of the Cortaderas lineament, Miocene to Holocene back-arc magmatic rocks are essentially absent and perhaps it marks the southern boundary of a transient Miocene shallow subduction zone (Kay et al., 2006). Thick sedimentary sequences and variable intraplate to arc-like chemical signatures in the volcanic rocks have been interpreted to reflect extensive lithospheric thinning in fore-arc and intra-arc basins (Muñoz et al., 2000). The Nazca plate that is currently subducting at this latitude corresponds to chrons 8–13 (ca. 33–25 Ma (Cande and Kent, 1992)). The Holocene centers of the transitional Southern Volcanic Zone segment to the north erupts dominantly andesitic lavas, whereas those of the southerly Southern Volcanic Zone segment are dominated by high-Al basalts (Stern, 2004).

Pre-Pliocene volcanic rocks of the Sierra de Huantraico region were dated by Kay and Copeland (2006) to be Early to Middle Miocene in age. The Desfiladero Negro dikes have an age of 25 ± 8 Ma (2σ), a flow in the Filo Morado ridge was dated to 23.4 ± 0.8 Ma (2σ). Amphibole phenocrysts from a mafic andesite flow near the southern end of the Huantraico syncline were dated to 19.8 ± 1.4 Ma (2σ). Cobbold and Rossello (2003) determined additional $^{40}Ar/^{39}Ar$ ages for a basalt flow from the Filo Morado ridge (22.2 ± 0.5 Ma), a flow (22.1 ± 0.5 Ma) and a dike (18.9 ± 0.4 Ma) just west of Cerro Bayo de Sierra Negra and five ages ranging from 16.1 ± 0.2 to 15.2 ± 0.1 for dikes surrounding the Cerro Bayo de Negra. Kay and Copeland (2006) divide the volcanic rocks into three groups based on their age determinations: (1) a Late Oligocene to Early Miocene Filo Morado basaltic sequence (24–20 Ma), (2) a younger Early Miocene Huantraico basaltic to andesitic sequence from the central and southern Sierra de Huantraico (20–18 Ma) and (3) a Miocene Cerro Villegas basalt (16–15 Ma). The Filo Morado basalts were described in detail by Kay and Copeland (2006) and include the alkali olivine basalt flows that crop out in the Sierra Negra and northern Sierra de Huantraico. Their age is >22.1 ± 0.5 Ma and their chemical characteristics overlap those of the La Matancilla flows (described below). We do not consider the Filo Morado basalts to be part of Huantraico plateau and they will not be discussed further here. The Huantraico sequence include basaltic to andesitic flows, sills and dikes in the southern and central Sierra de Huantraico area but not the older Desfiladero Negro dike unit described by Ramos and Barbieri (1988).

3. Analytical techniques

3.1. $^{40}Ar/^{39}Ar$ age determinations

Samples for radiometric dating were crushed to a 250–400 μm size fraction and were cleaned in a 2% hydrochloric acid solution to remove possible traces of weathered material. To make the contribution of magmatic argon and weathered phases negligible, phenocrysts were removed using magnetic separation methods and finally handpicking under an optic microscope, leaving only groundmass to be analyzed. Ar was measured from at least two different aliquots of the same groundmass preparation. The $^{40}Ar/^{39}Ar$ geochronology laboratory at the University of Lund uses a Micromass 5400 mass spectrometer with a Faraday and an electron multiplier. It is equipped with a metal extraction line, containing two SAES C50-ST101 Zr–Al getters and a cold finger cooled to app. −155 °C by a Polycold P100 cryogenic refrigeration unit. Samples were loaded into a copper planchette that consists of several 3 mm holes and step-heated using a defocused 50 W CO_2 laser. Sample clean-up time is 5 min (using two hot Zr–Al getters and a cold finger). The laser was rastered over the samples to provide even heating of all grains. The analytical process is automated and runs on a Macintosh OS 10.2 platform with software modified specifically for the laboratory at the University of Lund. Time zero regressions were fitted to data collected from 10 scans over the mass range of 36 to 40. Peak heights and backgrounds were corrected for mass discrimination, isotopic decay and interfering nucleogenic Ca-, K-, and Cl-derived isotopes. Blanks were measured before each sample and after every three sample steps. Blank values were subtracted from the sample signal for all incremental steps. Age plateaus were determined following the

Table 1
Results of $^{40}Ar/^{39}Ar$ analysis of groundmass separates.

Sample	Location	Plateau age				Inverse isochron age			Total fushion age	Geographical position	
		N/N^{tot}	Age ± 2σ Ma	^{39}Ar (%)	MSWD	Age ± 2σ Ma	$^{40}Ar/^{36}Ar$	MSWD	Age ± 2σ Ma	S	W
Huantraico											
127050 (#14)	Lower Series	4/11	17.90 ± 0.50	49.0	2.72	16.60 ± 0.50	299 ± 8	3.30	16.40 ± 0.4	37°27.635'	69°45.753'
127062 (#2)	Lower Series	6/12	17.80 ± 0.02	59.7	1.92	17.60 ± 0.20	295 ± 2	0.87	17.40 ± 0.3	37°27.584'	69°46.063'
127071 (#20)	Upper Series	10/10	17.61 ± 0.09	100.0	1.58	17.58 ± 0.06	299 ± 4	1.50	17.64 ± 0.13	37°33.630'	69°40.418'
La Matancilla											
127085		3/11	21.00 ± 0.20	44.9	2.81	n.c.	n.c.	n.c.			
126181		5/11	21.20 ± 0.30	38.2	3.42	20.40 ± 0.20	306 ± 10	1.60	20.60 ± 0.20	36°45.355'	69°07.169'
127077		5/11	24.27 ± 0.19	42.9	2.42	24.40 ± 0.30	307 ± 7	9.00			
Payunia											
126218	Co. las Yeguas	6/11	4.03 ± 0.16	50.0	1.58	4.40 ± 0.30	294 ± 10	5.90	3.70 ± 0.20	36°14.510'	68°40.938'
123946	Payunia	n.o.	n.o.	n.o.	n.o.	2.94 ± 0.11	271 ± 6	0.37	3.77 ± 0.11	36°41.711'	68°45.175'
123908	Patahuliloso	3/8	1.10 ± 0.20	46.5	2.58	n.c.	n.c.	n.c.	0.90 ± 0.30	35°46.009'	69°19.056'
Smaller volcanic centers											
127319	Huaiquaria	7/8	0.32 ± 0.14	84.3	1.47	n.c.	n.c.	n.c.	0.50 ± 0.20	34°04.523'	69°44.091'

Accepted ages are underlined. Also given are number of increments included in the age calculation, % of ^{39}Ar released from the sample and included in the age calculation and Mean Square Weighted Deviation (MSWD) for plateau and isochron age calculations. For the inverse isochron calculation the $^{40}Ar/^{36}Ar$ ratio is also given. Total fusion ages are reported for all samples and geographic locality is quoted in degrees decimal minutes (dd°mm.mmm′). See text for further discussion. N.c. = not calculated. N.o. = not obtained. Numbers in parantheses denote stratigraphic position of Huantraico samples.

criteria of Dalrymple and Lanphere (1971), specifying the presence of at least three contiguous incremental heating steps with statistically indistinguishable ages and constituting more than 50% of the total ^{39}Ar released during the experiment. Sanidine standard TCR with an assumed age of 28.34 Ma (Renne et al., 1998) was used as flux monitor. J-values were calibrated with a precision of 0.25%. Samples were irradiated at the Petten reactor. New radiometric ages are presented in Table 1.

3.2. Nd–Sr–Pb isotope analyses

Rock chips were leached for 1 h in hot 6 M HCl and dissolved in HF + HNO_3 (5:1). Pb was complexed in a mix of 1.5 M HBr and 2 M HCl and passed through ion exchange columns using AG1 × 8, 100–200# Biorad© resin. Elution was with 1 M HBr and 2 M HCl and Pb was extracted with 8 M HCl. Pb isotopic analyses were performed in the static mode on a VG 54–30 MC-TIMS at the Department of Geography and Geology, University of Copenhagen. Pb was measured using the $^{207}Pb/^{204}Pb$ double spike technique of Baker et al. (2004). Pb was loaded on Re filaments in silica gel and phosphoric acid. Loading and spiking was carried out according to Thirlwall (2000). An appropriate part of the sample (depending on the absolute Pb content) was loaded and from the intensity of the ^{206}Pb of the unspiked run, the appropriate amount of sample necessary for the spiked measurement was calculated. We aim for a $^{204}Pb/^{206}Pb$ ratio of 0.5–2 in the sample–spike mixture. The calculated sample amount was mixed and homogenized with 2 μl of spike, Si-gel and H_3PO_4 before loading. Filament temperatures range from 1150 to 1300 °C. At least one international standard (NBS981) was run with each sample batch. The running mean throughout the analyzing period (2010–2012) for NBS981 was 16.9390 ± 0.0029, 15.4992 ± 0.0038 and 36.7234 ± 0.0117 for $^{206}Pb/^{204}Pb$, $^{207}Pb/^{204}Pb$ and $^{208}Pb/^{204}Pb$ respectively (quoted at the 2σ confidence level and N = 35). Total chemical procedure blanks were 50–200 pg, insignificant compared to the >6 ng dissolved sample Pb. Sr was extracted using a cut from 2 M HCl passing through the anion exchange columns and cleaned using Sr-spec©. REE were collected from the columns after Sr and Nd was extracted from the REE fraction by ion exchange on Teflon-coated resin using 0.25 HCl. Sr was loaded in 1 M phosphoric acid and Ta slurry on Re filaments and Nd was loaded in 0.1 M HCl on Ta filaments in a triple filament arrangement with a center Re filament to ensure high T (1850–1900 °C) ionization. Sr and Nd were run dynamically and Sr results were corrected for mass fractionation using the exponential law and $^{86}Sr/^{88}Sr = 0.1194$. Nd was exponentially corrected to $^{146}Nd/^{144}Nd = 0.7219$. One standard, NBS987 and JNdi for Sr and Nd respectively, were run with each sample batch. The mean of 53 runs of JNdi and 60 runs of NBS987 during the analyzing period (2010–2012) yields 0.512096 ± 0.000016 (2σ) and 0.710241 ± 0.000019 (2σ) respectively. Age corrections of Early Miocene isotope ratios are applied. Isotopic ratios of Pb, Sr and Nd are presented in Table 2.

Table 2
Isotopic composition of Huantraico and La Matancilla lavas.

Sample	SiO_2	$^{87}Sr/^{86}Sr$	$^{143}Nd/^{144}Nd$	$^{206}Pb/^{204}Pb$	$^{207}Pb/^{204}Pb$	$^{208}Pb/^{204}Pb$
Huantraico						
127050	45.99		0.512915	18.4545	15.5307	38.1027
127057	50.35	0.703341	0.512909	18.5822	15.5796	38.3297
127063	50.10	0.703262	0.512915	18.4399	15.5667	38.1374
127069	50.90	0.703474	0.512875	18.5314	15.5741	38.2709
127072	55.25	0.703534	0.512862	18.5481	15.6064	38.3642
La Matancilla						
127083	48.81	0.704033	0.5127681	18.4095	15.6059	38.3706

3.3. Major and trace elements

28 volcanic rocks from the Huantraico plateau and 13 volcanic rocks from the La Matancilla plateau were analyzed for major and trace elements. All samples were treated in 0.5% HCl in order to remove secondary calcite (caliche) before jaw crushing. Jaw crushed material was powdered in an agate swing mill and thin sections were made of each rock for petrographic studies. Major elements were analyzed at the Rock Chemistry Laboratory at GEUS following the procedure described by Kystol and Larsen (1999). The elements Si, Al, Mg, Ti, Fe^{tot}, Mn, Ca, K and P were analyzed in sodium tetraborate glass tablets by X-ray fluorescence (XRF) on a Phillips PW 1606 spectrometer. The rock powder was heated in order to determine the volatile content (measured as loss on ignition). Na was analyzed by atomic absorption spectrometry (AAS) on a Perkin Elmer PE2280. The analytical precision of the data is (1σ, absolute wt.%) SiO_2: 0.15, TiO_2: 0.015, Al_2O_3: 0.05, $Fe_2O_3^{tot}$: 0.1, MnO: 0.003; MgO: 0.05, CaO: 0.03, Na_2O: 0.05, K_2O: 0.005, P_2O_5: 0.005, and volatiles: 0.1. Trace element measurements were also performed at GEUS by inductively coupled plasma mass spectrometry (ICP-MS) following a modified procedure of Ottley et al. (2003). The international standards BHVO-2 and BCR-2 and internal standard DISKO-1 were used to monitor the analytical quality and were dissolved and analyzed along with the samples. Results of internal and international standards are listed in the online Appendix A. Representative major and trace elements are presented in Table 3 and all analyzed samples are listed in the online Appendix B.

4. Sampling and petrography

La Matancilla lavas constitute a volcanic plateau, covering approximately 400 km^2, south of the Payún Matrú volcano. The plateau is approximately 20 km in diameter (E–W) and lavas were collected both from the lower parts of the plateau in two well exposed profiles and from lava flows on top of the plateau. At least 15 lava flows are exposed, varying in thickness from a few to tens of meters. La Matancilla lavas contain abundant olivine and clinopyroxene (5–20 vol.%) and sometimes plagioclase phenocrysts (<5 vol.%). In the otherwise well-preserved lavas olivine is often almost completely altered to iddingsite and often found as glomerocrysts. Olivine crystals are 1/2–1 mm in diameter. Clinopyroxene occurs as anhedral grains, rarely more than 1 mm in diameter. When plagioclase occurs as a phenocryst phase it is tabular or acicular, fresh and up to 1.5 mm in length. The matrix is dominated by plagioclase.

Huantraico lavas and dikes were sampled from the southern well-preserved parts of the Huantriaco plateau. Two main profiles, constituting app. 200 m of lavas, were collected on the western and southeastern margins of the plateau and on the eastern margin several dikes were sampled (Fig. 1). Most Huantraico lavas appear fresh in both hand specimen and thin sections. Nearly all phenocrysts are unaltered, except for olivine in some samples, which have rims of iddingsite and amphibole that commonly has a rim of oxides. The groundmasses appear unaltered. Basaltic to basalt andesitic flows, sills and dikes in the southern and western Huantraico region as well as evolved clinopyroxene-bearing basalt and clinopyroxene–hornblende-bearing basaltic andesitic flows and dikes, are included in the Huantraico sequence. The most primitive olivine- and clinopyroxene bearing basalts crop out in the central and western part of the Sierra de Huantraico (*Huantraico Lower Series*, HLS) (Fig. 1D–E). More evolved clinopyroxene and hornblende bearing basalts to trachyandesites (*Huantraico Upper Series*, HUS) crop out in the prominent cliffs at the southeastern end of the Sierra de Huantraico (Fig. 1e) and petrographically and geochemically similar outcrops are found as eroded centers on the plateau (described by Kay and Copeland, 2006). Plagioclase is the most abundant phenocryst and present in all Huantraico samples. Olivine is the first occurring mafic phase (present in all samples with MgO > 5 wt.%). It occurs as individual phenocrysts and in clusters and is typically 1/2–2 mm in diameter.

Table 3
Representative major and trace element analyses of Huantraico and La Matancilla lavas.

Sample	127050	127051	127057	127058	127062	127063	127064	127069	127070	127071	127072	127073	127074	127077	127078	127079	127083	127084	127086	126181
	HLS	HLS	HLS	HLS	HLS	HLS	H. dike	HUS	HUS	HUS	HUS	HUS	HUS	Mat.	Mat.	Mat.	Mat.	Mat.	Mat.	Mat.
SiO_2 (wt%)	45.99	48.47	50.35	49.60	48.11	50.10	53.38	50.90	53.78	55.27	55.25	55.32	51.22	48.41	48.12	48.70	48.81	58.10	48.86	47.05
TiO_2	1.38	1.67	1.79	1.38	1.43	1.30	1.26	1.28	0.98	1.13	1.13	1.22	1.37	2.08	1.73	1.70	1.88	0.88	2.51	2.17
Al_2O_3	14.22	16.54	17.50	19.19	17.70	20.33	19.37	19.63	17.26	18.31	18.34	19.17	18.93	15.04	14.75	14.91	15.23	18.61	16.85	15.19
FeO^{tot}	10.49	9.83	9.30	9.50	9.68	8.62	7.91	7.84	8.06	6.49	6.41	6.94	8.71	11.40	10.61	10.45	10.38	6.37	9.73	10.87
MnO	0.17	0.17	0.14	0.13	0.18	0.17	0.14	0.19	0.18	0.17	0.17	0.08	0.20	0.16	0.15	0.15	0.15	0.18	0.15	0.16
MgO	12.13	7.05	4.01	4.27	6.39	3.33	1.77	3.43	3.72	1.99	1.99	1.54	3.57	6.77	7.56	8.18	7.02	1.00	4.19	6.40
CaO	11.05	10.12	10.25	10.11	11.09	9.48	7.95	9.72	8.87	8.02	8.11	6.74	8.67	9.15	10.86	9.69	9.92	3.19	9.05	10.11
Na_2O	2.45	3.12	3.43	3.43	2.80	3.67	4.47	3.81	3.74	4.51	4.50	4.69	3.73	3.70	3.51	3.56	3.75	6.67	4.56	3.81
K_2O	0.56	1.48	1.75	1.03	1.10	1.57	2.37	1.84	2.13	2.90	2.90	3.03	2.15	1.45	1.08	1.09	1.22	3.76	2.19	1.25
P_2O_5	0.39	0.44	0.45	0.30	0.42	0.47	0.51	0.47	0.37	0.50	0.49	0.49	0.48	0.56	0.44	0.41	0.48	0.53	0.82	0.46
Sum	98.83	98.90	98.96	98.94	98.92	99.04	99.12	99.13	99.10	99.28	99.29	99.23	99.03	98.73	98.82	98.84	98.84	99.29	98.92	97.48
LOI	1.8	2.2	3.7	2.7	2.6	2.1	3.8	2.1	2.0	2.8	2.8	2.2	2.5	2.6	1.9	1.0	2.2	1.6	0.5	1.2
Sc (ppm)	32.85	23.77	24.14	21.05	26.66	12.04	14.32	16.70	17.55	12.20	12.38	13.91	15.94	21.77	21.77	19.21	19.52	7.17	20.37	22.05
V	273.88	264.81	249.24	245.91	260.44	173.58	172.16	197.79	170.30	149.06	153.61	161.36	223.28	195.02	207.31	161.33	169.14	8.97	277.68	205.74
Cr	665.09	171.12	61.46	12.57	95.61	2.27	3.41	16.12	68.08	11.72	10.31	12.82	3.78	314.67	317.73	295.84	270.71	0.39	40.65	209.95
Co	57.84	37.58	28.51	32.40	36.31	24.49	20.72	22.96	25.02	18.09	19.06	15.16	26.22	45.88	50.98	48.72	44.51	5.86	30.91	44.75
Ni	246.66	84.77	31.18	20.92	46.71	8.04	12.09	12.10	28.11	9.83	10.37	10.31	7.88	191.14	228.54	223.87	196.77	1.66	30.84	113.26
Cu	67.23	65.64	62.69	39.37	45.86	50.20	42.83	45.01	52.68	20.61	21.56	33.13	48.68	49.09	45.11	45.40	51.55	7.57	36.24	49.76
Zn	78.55	80.86	87.92	70.33	75.66	76.68	71.96	70.69	75.06	68.51	69.12	71.06	80.02	102.59	97.02	90.30	90.97	68.10	101.66	102.03
Ga	18.23	21.02	20.93	19.34	19.44	20.59	21.71	21.39	19.23	20.46	21.36	21.74	21.68	21.40	20.45	19.77	20.95	23.54	24.48	22.32
Rb	13.14	31.21	44.27	17.79	20.99	28.14	48.54	37.98	48.65	62.78	64.89	63.18	47.19	16.11	14.00	14.22	16.56	54.69	21.51	12.64
Sr	760.36	831.45	685.71	686.54	832.85	973.58	742.65	871.88	753.79	730.97	767.72	717.39	853.59	736.44	629.40	571.85	597.45	555.26	979.62	1021.48
Y	20.23	23.12	23.27	20.52	22.10	25.24	23.74	23.93	22.54	26.28	26.80	25.13	28.77	20.86	18.82	18.19	20.32	24.55	23.78	21.32
Zr	109.69	138.22	141.99	97.29	111.36	122.66	182.40	133.91	178.44	200.10	205.45	207.52	163.05	183.46	156.05	148.44	170.52	451.80	245.62	166.19
Nb	14.57	20.21	20.04	11.69	16.17	17.77	24.68	17.49	21.23	26.15	27.05	27.00	21.82	36.16	26.00	23.84	27.97	67.05	47.53	24.92
Cs	0.67	0.50	0.89	0.13	0.21	0.18	0.22	0.50	1.47	1.11	1.15	0.67	0.78	0.21	0.10	0.15	0.16	1.27	0.35	0.17
Ba	217.74	323.35	354.42	178.65	215.19	251.47	452.86	369.07	401.50	518.06	535.78	505.54	385.79	312.82	247.10	266.97	252.54	728.05	589.40	311.94
La	16.20	19.95	18.79	12.35	15.68	17.47	25.48	21.12	22.73	26.83	27.64	27.01	22.98	25.19	19.87	18.57	21.31	51.61	33.21	20.53
Ce	35.77	42.37	40.99	27.99	34.34	38.96	51.59	45.38	46.87	55.39	56.62	55.60	49.57	52.30	41.69	38.39	44.71	97.99	67.49	43.89
Pr	4.97	5.74	5.69	3.95	4.80	5.52	6.62	5.76	5.80	6.67	6.86	6.85	6.32	6.54	5.24	4.89	5.60	10.50	8.58	5.53
Nd	22.22	24.64	24.89	18.18	21.39	25.15	27.72	24.85	24.04	27.52	28.21	28.43	27.59	27.80	22.65	21.37	24.03	37.20	34.88	24.53
Sm	5.13	5.63	5.51	4.08	4.82	5.63	5.86	5.34	4.87	5.82	5.97	5.88	6.06	5.94	4.97	4.72	5.36	6.02	7.31	5.49
Eu	1.67	1.83	1.76	1.36	1.57	1.88	1.88	1.72	1.48	1.74	1.82	1.78	1.93	1.92	1.70	1.59	1.77	1.82	2.25	1.80
Gd	4.99	5.52	5.46	4.25	4.75	5.67	5.69	5.28	4.68	5.57	5.75	5.57	5.97	5.65	4.81	4.55	5.16	5.38	6.87	5.59
Tb	0.724	0.820	0.793	0.671	0.730	0.852	0.809	0.783	0.704	0.837	0.853	0.820	0.908	0.844	0.721	0.679	0.762	0.821	0.948	0.786
Dy	3.85	4.51	4.60	3.76	4.18	4.71	4.71	4.38	4.00	4.60	4.74	4.57	5.10	4.28	3.75	3.62	4.04	4.39	4.91	4.19
Ho	0.69	0.80	0.82	0.72	0.79	0.88	0.86	0.86	0.79	0.90	0.92	0.88	1.01	0.76	0.71	0.68	0.75	0.84	0.86	0.74
Er	1.88	2.17	2.20	2.00	2.16	2.45	2.31	2.23	2.19	2.48	2.52	2.41	2.74	1.93	1.74	1.68	1.92	2.41	2.25	2.00
Tm	0.26	0.31	0.31	0.30	0.31	0.37	0.34	0.33	0.34	0.37	0.39	0.36	0.41	0.26	0.25	0.24	0.26	0.37	0.30	0.25
Yb	1.56	1.88	2.00	1.85	1.94	2.18	2.14	2.12	2.12	2.35	2.46	2.10	2.55	1.54	1.45	1.41	1.57	2.39	1.72	1.51
Lu	0.23	0.28	0.28	0.28	0.30	0.33	0.31	0.31	0.34	0.37	0.38	0.33	0.38	0.23	0.20	0.20	0.22	0.37	0.25	0.23
Hf	2.683	3.311	3.461	2.367	2.727	2.940	4.141	3.102	3.968	4.433	4.548	4.626	3.665	4.081	3.465	3.376	3.864	8.809	5.210	3.719
Ta	0.855	1.181	1.193	0.671	0.934	1.057	1.504	1.027	1.355	1.652	1.707	1.737	1.312	2.051	1.460	1.348	1.575	4.091	2.805	1.463
Pb	2.725	3.894	4.295	2.383	2.567	3.521	5.799	4.268	4.645	4.246	4.398	5.928	4.811	2.705	2.479	2.575	2.502	6.777	3.990	2.186
Th	2.070	2.854	2.631	1.352	1.943	2.320	4.650	3.082	4.816	5.537	5.723	5.750	3.820	2.588	2.175	2.025	2.327	7.943	3.629	2.253
U	0.57	0.90	0.68	0.41	0.53	0.71	1.46	0.97	1.59	1.87	1.96	1.76	1.24	0.88	0.51	0.59	0.64	2.25	1.09	0.56
Eu/Eu^*	1.00	0.99	0.97	0.99	0.99	1.01	0.98	0.98	0.93	0.92	0.94	0.94	0.97	1.00	1.05	1.03	1.01	0.96	0.96	0.99
Longitude (W)	69.763	69.763	69.763	69.763	69.768	69.768	69.629	69.672	69.673	69.674	69.674	69.675	69.675	69.469	69.469	69.482	69.479	69.442	69.378	69.120
Latitude (S)	37.461	37.461	37.459	37.459	37.460	37.460	37.525	37.561	37.561	37.561	37.560	37.560	37.560	36.811	36.811	36.839	36.839	36.659	36.645	36.756

H. dike = dike cutting the Huantraico plateau.
Mat. = La Matancilla lavas.

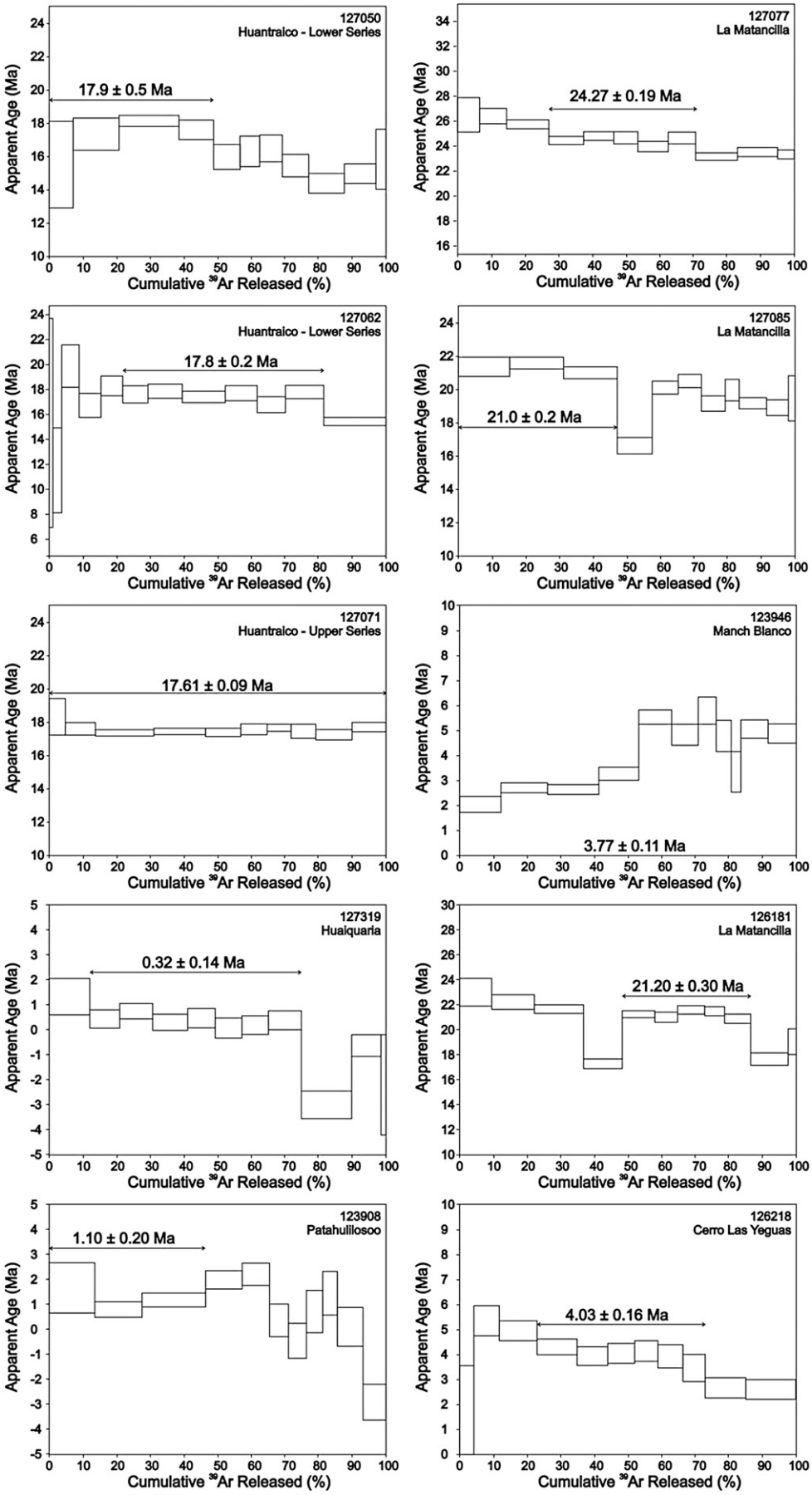

Fig. 2. Age plateaus for Huantraico, La Matancilla and younger samples. See text for interpretations.

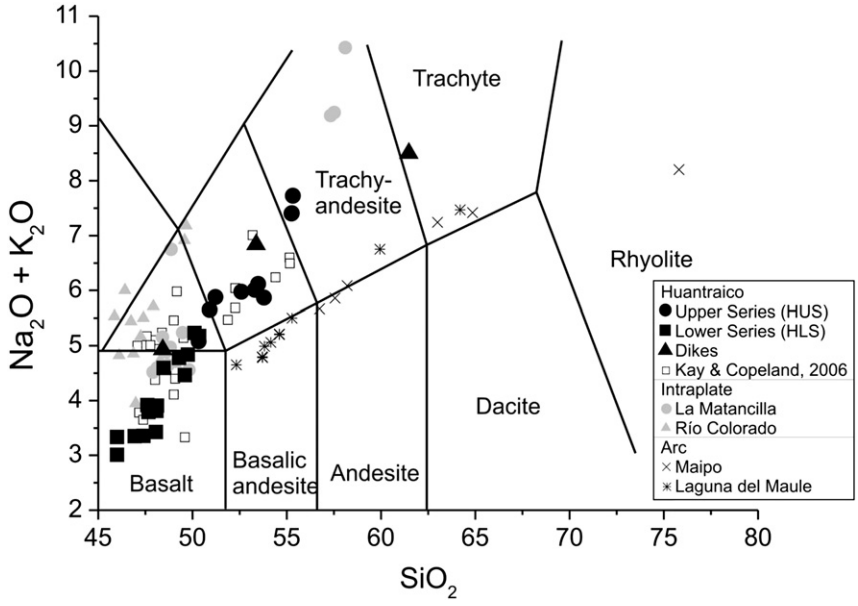

Fig. 3. HLS lavas are mainly basalts with a few trachybasalts (hawaiites). HUS generally have higher contents of alkalis and silica, ranging from hawaiite through mugearites to benmoreites (Le Maitre, 2002). Also shown are Huantraico literature data (Kay and Copeland, 2006) as well as intraplate-like Río Colorado lavas (Søager et al., 2013) and arc lavas from two volcanoes, Maipo and Laguna del Maule (Holm et al., in preparation).

Clinopyroxene is rare but occurs in most samples belonging to HLS as small anhedral grains (<1 mm). Amphibole is the last mafic phase to crystallize and replaces clinopyroxene toward the top of the Upper Series. Amphibole is generally rimmed by oxides and only found as individual grains varying in size from 1 to 2 mm. The matrix is composed of plagioclase ± olivine ± clinopyroxene.

Several younger lava flows have also been collected in order to better constrain the temporal variation across the area. This includes samples from Huaiquaria, Patahuliloso, Cerro Las Yeguas and Payenia. The Huaiquaria region is dotted with several small cones, all assumed to be of similar age. The small volcanic shield, Patahuliloso, is constructed of several pahoehoe flows. The collected sample (123908) is from the southern rim and is assumed, based on field relations, to be the youngest flow from this volcanic center. The Nevado volcanic field is characterized by highly eroded cones and is of Late Pliocene–Pleistocene age (Bermúdez and Delpino, 1989; Gudnasson et al., 2012; Muñoz et al., 1989). Cerro Las Yeguas is shown to be of Early Pliocene age, extending the volcanic activity of the Nevado Field slightly. Several large pahoehoe flows extend from the Payún Matrú volcano towards the east. Also, the volcanic plateau underlying the Payún Matrú volcano has been dated.

5. Results

5.1. Geochronological data

Ten new $^{40}Ar/^{39}Ar$ radiometric ages range from ~22 Ma to 0.32 Ma for back-arc samples. Age plateaus are shown in Fig. 2 and results are listed in Table 1. In addition to Huantraico lavas and La Matancilla lavas, ages of volumetrically small volcanic occurrences in Huaiquaria and Payenia are reported.

5.1.1. Huantraico plateau

Three samples from the southern cliffs of the Sierra de Huantraico yield Burdigalian ages of 17–18 Ma. These ages are in accordance with previous age determinations (e.g. Kay and Copeland, 2006).

5.1.1.1. Huantraico Lower Series (HLS). Sample 127050 was collected in the uppermost part of HLS. A plateau age of 17.9 ± 0.5 Ma, including four adjacent steps and 49% of the released ^{39}Ar, is assumed to be overestimating the geological age of the sample slightly as the 7 high-temperature steps are around 16 Ma. A satisfying lower plateau is not

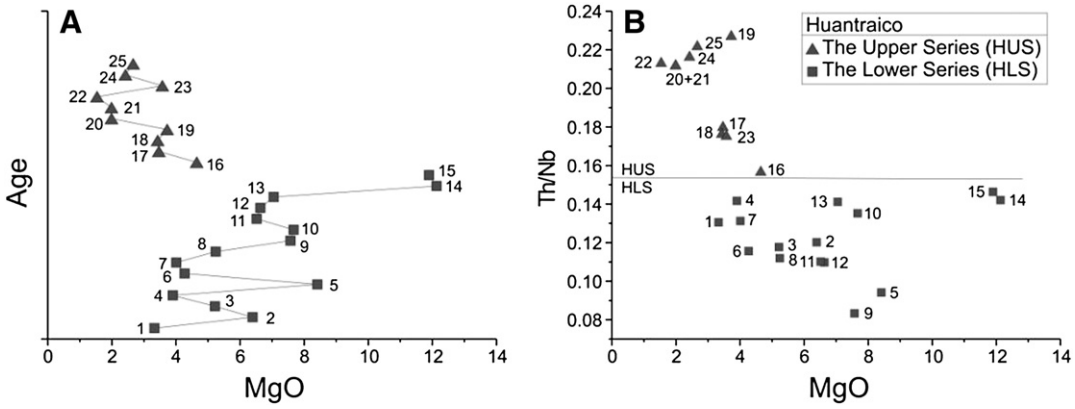

Fig. 4. A) Relative height above the surrounding plains of 25 lavaflows vs. MgO content show an overall increase in MgO with respect to time throughout the Lower Series although major inflections are apparent evidencing that the lavas are not comagmatic although likely to have originated from similar sources. The same holds true for the Upper Series, however an overall decrease in MgO with time is apparent. B) Distinct differences in very incompatible trace element ratios evidence that fractional crystallization processes alone cannot explain all variation in Huantraico lavas.

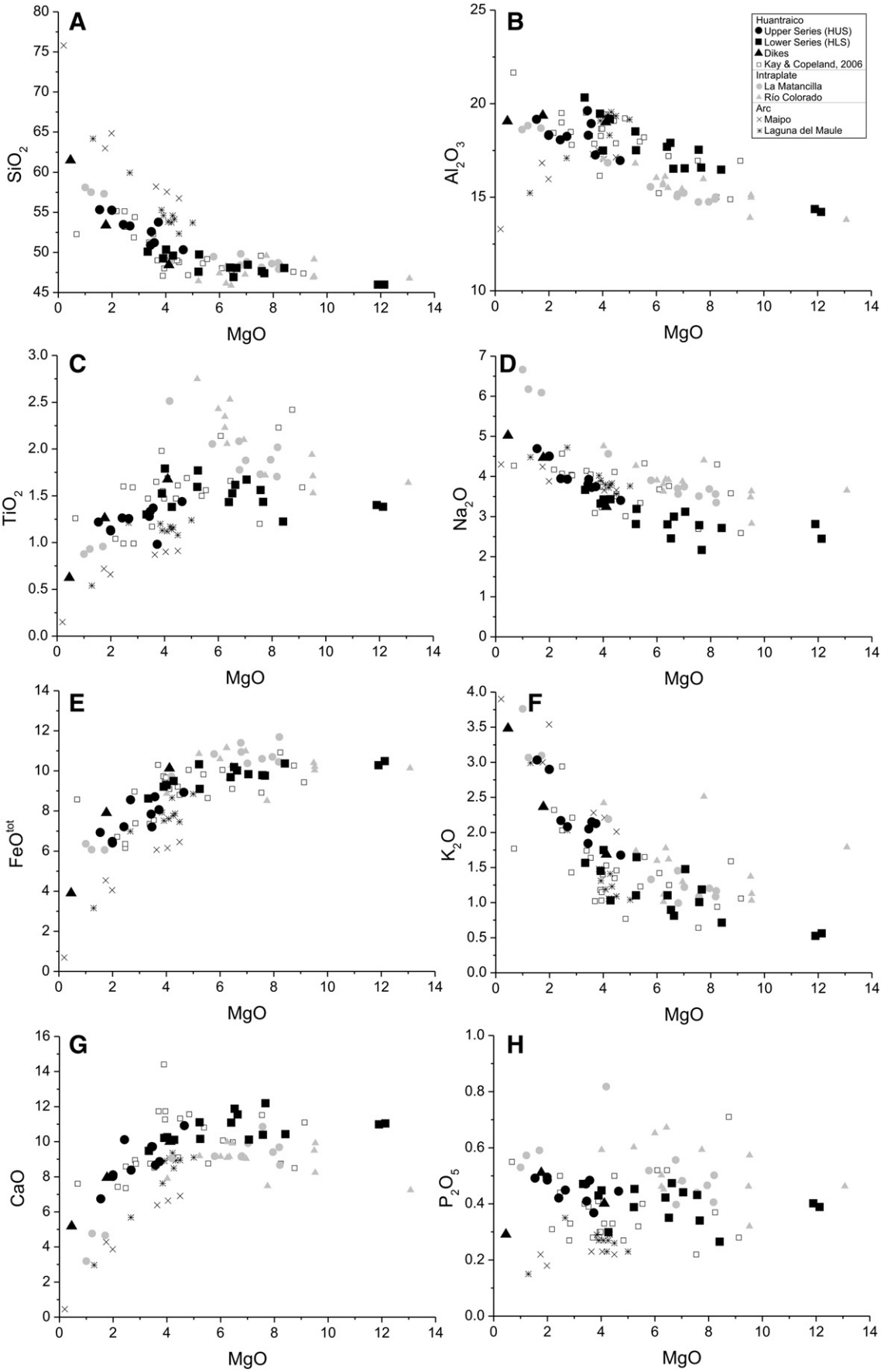

Fig. 5. Variation diagrams for major elements (wt.%) vs. MgO (wt.%). Data sources as in Fig. 3.

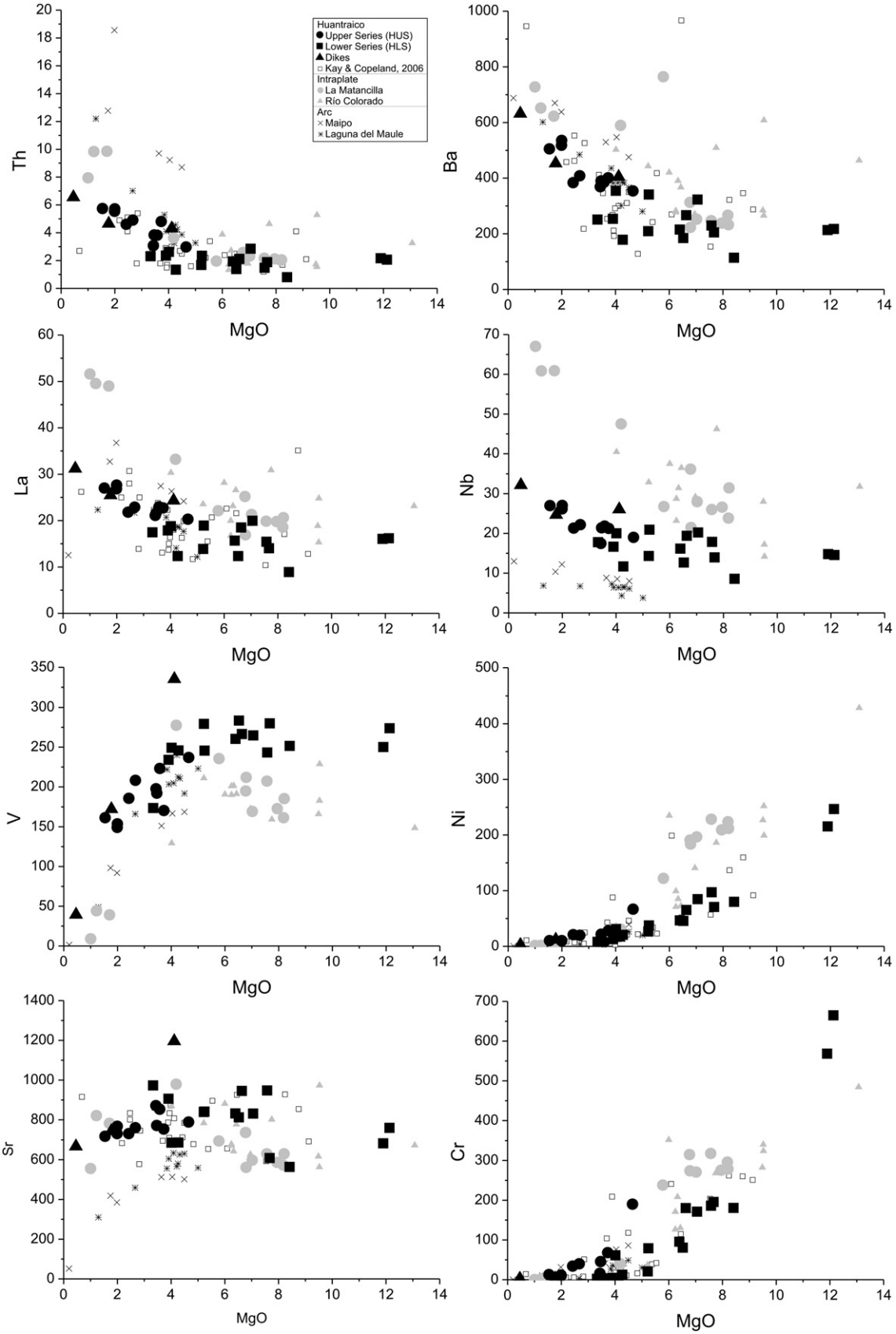

Fig. 6. Selected trace elements (ppm) vs. MgO (wt.%). Data sources as in Fig. 3.

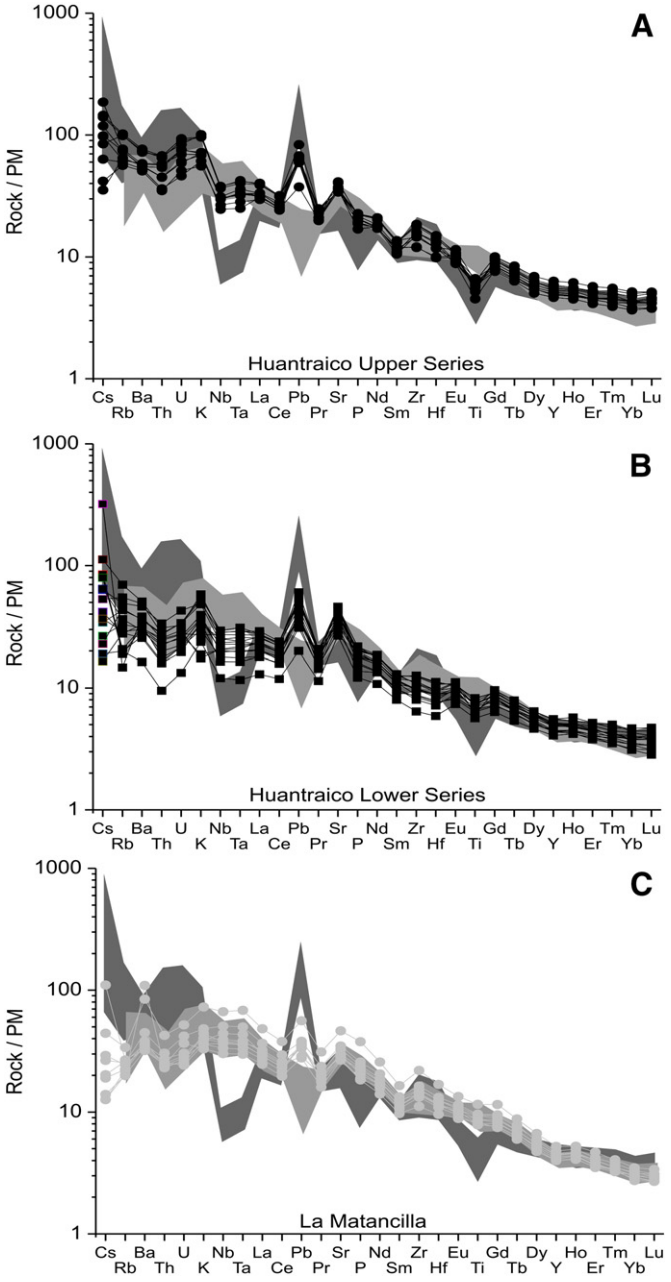

Fig. 7. Mantle normalized trace element compositions of Huantraico lavas and La Matancilla lavas compared with Quaternary Andean Orogenic arc basalts from the Laguna del Maule volcano (dark gray field) (Frey et al., 1984; Holm et al., in preparation) and back-arc basalts showing an OIB-like signature from Río Colorado (light gray field) (Søager et al., in preparation). Note that Huantraico Upper Series (HUS) is generally enriched in incompatible elements with the exception of Ti with respect to Huantraico Lower Series (HLS). The positive Sr anomaly is more distinct in HLS than in HUS. Trace element patterns show behavior that is intermediate to arc and OIB with positive Pb and negative Ti resembling the Andean arc but also a very low negative Nb–Ta anomaly, a slight enrichment in LILE and positive Sr as observed in Río Colorado. Primitive mantle normalization is according to Sun & McDonough (1989).

obtained. The total fusion age is 16.4 ± 0.4 Ma and in accordance with the isochron age of 16.6 ± 0.5 Ma. The $^{40}Ar/^{39}Ar$ ratio is 299 ± 8. The plateau age is accepted as a maximum age for sample 127050.

Sample 127062, from the lower part of HLS is much better defined. A plateau age of 17.80 ± 0.02, defined by 6 steps and 59.7% of the released ^{39}Ar is confirmed by an inverse isochron age of 17.6 ± 0.2 Ma and accepted as representing the crystallization age of the lower parts of the Huantraico plateau. No excess argon is present in the sample ($^{40}Ar/^{39}Ar$ = 295 ± 2).

5.1.1.2. Huantraico Upper Series (HUS). A single sample, 127071, from the middle of HUS yields a plateau age of 17.61 ± 0.09 Ma (100% released ^{39}Ar included in the calculation). The inverse isochron age of 17.58 ± 0.06 confirms the plateau age. Within uncertainty, a maximum of only a few 100 ka separates the lower part of the volcanic plateau from the upper, implying that the vast Huantraico plateau was emplaced over a relatively short time period.

The quite narrow age range indicating perhaps as little as 17.5–17.8 Ma for the formation of the Huantraico plateau in southern Huantraico overlaps with age determinations of a dyke W of nearby Cerro Bayo de Sierra Negra (Cobbold and Rossello, 2003), a Pichi Tril andesite (Ramos and Barbieri, 1988) and the Cerro Villagas flow just east of Huantraico (Kay and Copeland, 2006) at the 2σ uncertainty level, whereas most Cerro Bayo dikes of c. 15–16 Ma (Cobbold and Rossello, 2003) appear to be distinctly younger.

5.1.2. La Matancilla plateau

5.1.2.1. La Matancilla. Three samples from La Matancilla yield ages of 24–20 Ma for the volcanic plateau. Sample 127085, collected from the upper and central part of the La Matancilla plateau yields a plateau age of 21.0 ± 0.2 Ma but no isochron age due to a clustering of data points. Sample 126181 represents the easternmost flows covering an older volcanic plateau and extending several kilometers to the east from the main plateau. A plateau age of 21.2 ± 0.3 Ma is slightly higher than the inverse isochron age of 20.4 ± 0.2 Ma with a $^{40}Ar/^{36}Ar$ ratio of 306 ± 10. The plateau only includes 38% of the released ^{39}Ar and the isochron age is accepted as geologically significant. Sample 127077 from the southeastern cliffs reveals a plateau age of 24.27 ± 0.19 Ma and an inverse isochron age of 24.4 ± 0.3 Ma. A high $^{40}Ar/^{36}Ar$ ratio of 307 ± 7 indicates that 24.4 Ma must be considered a maximum age. The Matancilla plateau was constructed over a period of approximately 4 Ma.

Together with sample DRC21 (Kay and Copeland, 2006) our three new age determinations constitute a group of $^{40}Ar/^{39}Ar$ analyses with uncertainties around 0.2 Ma at the 95% confidence level, and these have a range of 20.2–24.5 Ma, which may span the activity of Matancilla volcanism, a range similar to the suggestion of Kay et al. (2006). Other $^{40}Ar/^{39}Ar$ and K–Ar analyses from Matancilla, Sierra Negra, Filo Morado, Desfiladero Negro and Cerro Tormenta SE of Huantraico (Cobbold and Rossello, 2003; Kay and Copeland, 2006; Perez and Condat, 1996; Ramos and Barbieri, 1988) which based on geology may be considered to be comtemporaneous with Matancilla volcanism, overlap this range if 2σ errors are considered.

5.1.3. Pliocene–Pleistocene samples

5.1.3.1. Huaiquaria. A well-defined plateau for sample 127319, constituting more than 80% ^{39}Ar yields an age of 0.32 ± 0.14.

5.1.3.2. Patahuliloso. A poorly defined plateau, comprising only 46.5% of the released ^{39}Ar reveals an age of 1.10 ± 0.20 Ma. The plateau is defined by low-temperature steps and high-temperature steps generally give lower ages. An isochron age has not been calculated as all data points plot very close to each other making it impossible to define an isochron. Due to low high-temperature steps and a total fusion age of 0.90 ± 0.30 Ma the plateau age is accepted as the maximum age of the Patahuliloso shield.

5.1.3.3. Cerro Las Yeguas. Sample 126218 is from a small lava flow on the flank of Cerro las Yeguas (Nevado Area). The plateau age defined on the $^{40}Ar/^{39}Ar$ step-heating spectrum diagrams is 4.03 ± 0.16 Ma. The last couple of steps have a slightly lower calculated age indicating that the plateau age should be considered a maximum age. This conclusion is supported by a second run of the sample (not shown) also showing a decrease in apparent age for the last couple of steps although a plateau

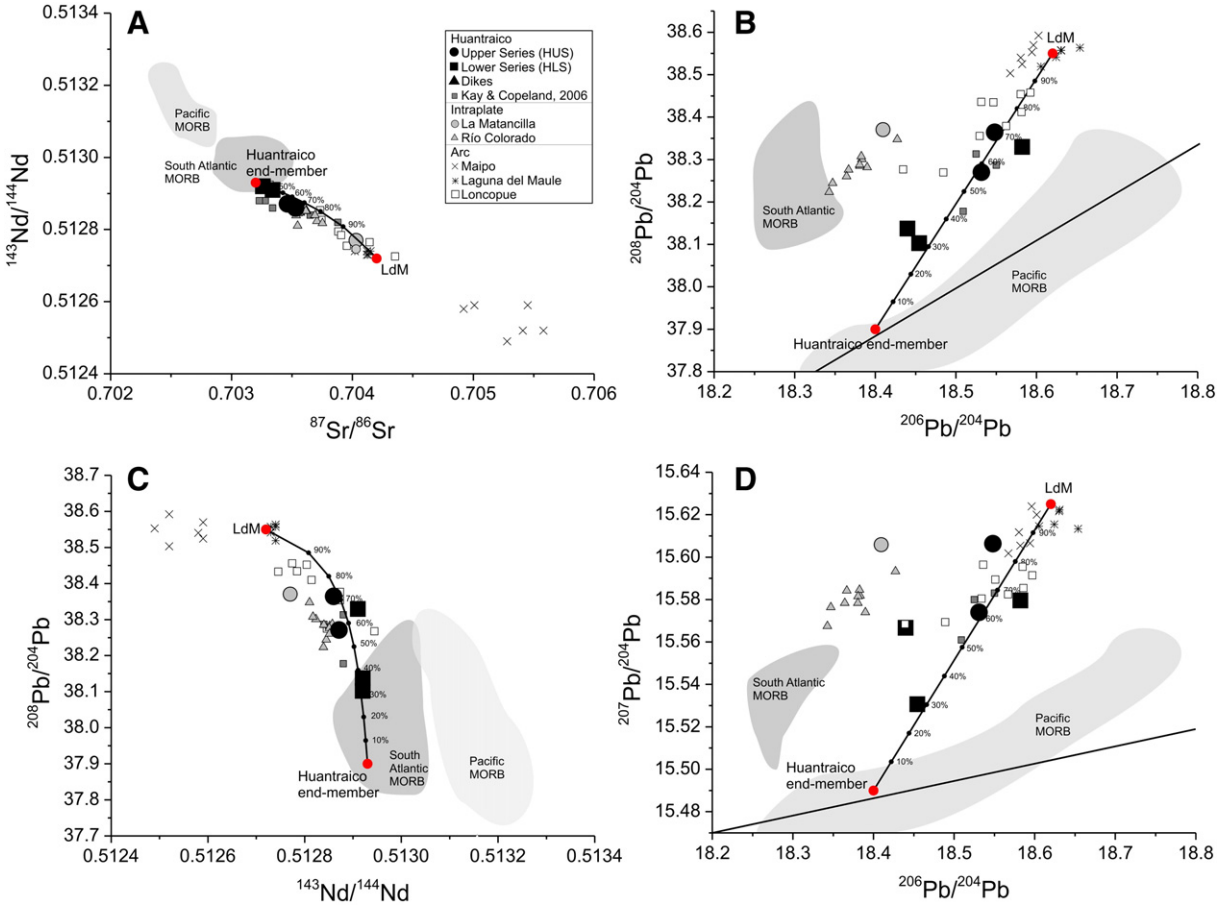

Fig. 8. Isotopic composition of Sr, Nd and Pb from Huantraico and La Matancilla. Also shown is the composition of Río Colorado, Maipo and Laguna del Maule. Río Colorado data are from Søager et al. (2013) and Holm et al. (in preparation). South Atlantic MORB field is from Le Roux, 2000 and Pacific MORB field is from White et al. (1987). The Sr, Nd and Pb abundance in the LdM (Laguna del Maule) source component is calculated assuming that Laguna del Maule lavas represent 10% melting and in the Huantraico source is assumed to be DMM (Stracke and Bourdon, 2009). The mixing model is based on Vollmer (1976). Loncopue data are from Varekamp et al. (2010).

is developed including 4 intermediate steps, revealing an age of 3.9 ± 0.3 Ma. When removing these steps from the inverse isochron calculation an age of 4.4 ± 0.3 is found and the $^{40}Ar/^{36}Ar$ ratio is 294 ± 10. However the scatter in the data is quite large resulting in a high MSWD value of 5.9 and the plateau age is accepted as the maximum age of 126218.

5.1.3.4. East of Payún Matrú. For sample 123946 no acceptable plateau age can be obtained and the inverse isochron age of 2.94 ± 0.11 Ma is assumed to underestimate the geological age of the lava flow, indicated by a $^{40}Ar/^{36}Ar$ ratio lower than in the atmospheric component. The total fusion age of 3.77 ± 0.11 Ma is accepted as best representing the crystallization age of the lava flow. A second sample from the lava flows underlying the Payún Matrú Volcanic Field to the east (126181) has a plateau age of 21.20 ± 0.30 Ma. This represents the volcanic basement on which Payún Matrú is built.

5.2. Major and trace elements

La Matancilla lavas (48–58 wt.% SiO_2) range from basalt to trachyandesite (Fig. 3) and represent magmatic episode 1 (24–20 Ma). Episode 2 (19–17 Ma) is represented by the Huantraico plateau rocks (46–62 wt.% SiO_2) ranging from basalt to trachyandesite (Fig. 3). The bulk of samples included in this study is sampled along two vertical profiles through the volcanic succession in the southern cliffs of the Huantraico plateau and are divided into two principal compositional and geographical groups (Fig. 4A). The Huantraico Lower Series (HLS) (flows 1–15) were collected in the western cliffs of the Huantraico plateau and are mainly subalkaline basalts (45–51 wt.% SiO_2). Increasing silica is accompanied by increasing alkalinity. Lavas of the Huantraico Upper Series (HUS) (flows 16–25), collected from the southeastern part of the plateau, are slightly more evolved (51–55.5 wt.% SiO_2), ranging from trachybasalt to trachyandesite. Trace element differences will be discussed further below. Dikes cut the Huantraico plateau (samples 127064, 065 and 066 in Fig. 1B). The lava flows range in thickness from a few to tens of meters and dip approximately 5°E. HLS lavas, collected in the western profile, are older than the ones from HUS along the eastern profile.

Whole-rock major and compatible trace element variations define coherent trends with MgO consistent with fractional crystallization for both the Upper and Lower Series (Fig. 5). The dataset shows a continuous evolution from basalt to trachyandesite, however this pattern is not correlated directly with the stratigraphy (Fig. 4A). Within the Lower Series the general trend is towards less evolved compositions with time, whereas the Upper Series shows a continuous evolution towards more MgO-poor compositions. There is an overall tendency that the Upper Series is more evolved than the Lower Series (higher SiO_2 and lower MgO). HLS shows a systematic increase in TiO_2 with decreasing MgO which is in contrast to HUS where TiO_2 decreases from 5 wt.% MgO. FeO, MnO and CaO all decrease with decreasing MgO (for both series) whereas SiO_2, Al_2O_3, K_2O, Na_2O and P_2O_5 increase with decreasing MgO (Fig. 5). Most of the Huantraico rocks are medium K_2O basalts (45–52 wt.% SiO_2), the exception being the basaltic andesites of the Upper Series. Huantraico lavas range widely in MgO content from 12 to 1 wt.%. A sharp decrease in CaO at 4 wt.% MgO, and relatively constant Al_2O_3 with decreasing MgO indicates a change from olivine-

dominated fractionating assemblages to plagioclase + clinopyroxene-dominated assemblages. Volatiles in the analyzed samples range from 0 to 3 wt.% and no samples show evidence of significant post magmatic alteration. Normative minerals were calculated using a Fe_2O_3/FeO ratio of 0.20 (Rollinson, 1993). Most lavas from the lower part of HLS are nepheline normative with a range from 0 to 3.6% normative ne content. The nepheline content decreases towards the top and above lava flow #5 most samples are hypersthene normative (0.2–10.1% hy). All lava flows have olivine in the norm.

Selected trace elements plotted against MgO are consistent with fractionation-related processes (e.g. decreasing Ni (250–0 ppm) and Cr (650–0) implying continuous fractionation of olivine ± clinopyroxene) (Fig. 6). Vanadium abundance is constant (~275 ppm) in the Lower Series and rapidly decreasing throughout the Upper Series. It also correlates positively with CaO (not shown). Most incompatible elements remain constant throughout HLS but show increasing trends with decreasing MgO in HUS (Fig. 7). There is a large gap in Nb content between the Andean arc volcanoes (represented by Maipo and Laguna del Maule) and the intraplate-like back-arc lavas represented by La Matancilla and Río Colorado. Huantraico lavas fill this gap with Nb contents ranging from 15 to 20 ppm at MgO = 7 wt.% (Fig. 6).

The REE distribution patterns normalized to Primitive Mantle (Sun and McDonough, 1989) are similar for HLS and HUS. Fig. 8 shows the primitive mantle normalized trace element compositions of both series compared to the Laguna del Maule stratovolcano erupted along the volcanic front of the Andean orogenic arc at 39°S and the Río Colorado/La Matancilla basalts, representing a Recent/Miocene OIB-like mantle source devoid of subduction components. HUS is generally enriched compared to HLS due in part to more extensive crystal fractionation (see below). However, the enrichment must also reflect a change in source composition as incompatible elements, such as La (Fig. 6), are enriched in HUS with respect to HLS at MgO = 4 wt.%, and very incompatible element ratios differ, e.g. Th/Nb is higher in HUS than in HLS (Fig. 4B). HUS presents some features similar to those observed in basalts from volcanic arcs, i.e. negative Ti and Pb anomalies. Lavas of HLS generally show concentrations and distribution patterns similar to OIB or MORB, e.g. a lack of a negative Nb–Ta anomaly.

5.3. Nd–Sr–Pb isotopes

Table 2 shows Nd, Sr and Pb (whole rock) isotopic ratios of selected samples from the Huantraico plateau, representing most of the stratigraphic sequence. These data are compared to young Andean volcanic rocks (Laguna del Maule and Maipo) as well as back-arc basalts to the north and the south of the study area (Río Colorado and Loncoupe) as well as previously published isotope data from the Huantraico region. The Sr isotopic composition of Huantraico ranges from 0.70323 to 0.70353 (Fig. 8) which is well within the Patagonian alkali basalts ranging from 0.70316 to 0.70512 (Stern et al., 1990). The Nd isotopic composition correlates inversely with the Sr isotopic composition (Fig. 8) and $^{143}Nd/^{144}Nd$ range from 0.51292 to 0.51286. Low Sr isotopic ratios cause Huantraico rocks to plot to the left of the array of Andean volcanic rocks on the $^{87}Sr/^{86}Sr$ vs. $^{143}Nd/^{144}Nd$ plot and a significant change towards more radiogenic Sr is noted from HLS to HUS with HUS plotting the farthest away from the MORB field. The Pb isotope ratios fall between MORB and local arc fields in $^{207}Pb/^{204}Pb$–$^{206}Pb/^{204}Pb$ and $^{208}Pb/^{204}Pb$–$^{206}Pb/^{204}Pb$ diagrams (Fig. 8B, D). $^{207}Pb/^{204}Pb$ and especially $^{208}Pb/^{204}Pb$ are lower at a given $^{206}Pb/^{204}Pb$ ratio than those of SVZ rocks similar to trends observed in the Loncoupe Graben (Varekamp et al., 2010).

La Matancilla and Río Colorado plot farther away from the MORB field than the Huantraico series but are positioned at relatively low Nd isotope ratios suggesting EM1 source component influences and are quite distinct from the SVZ-Huantraico suite. The combined isotope data suggest that at least three source components are responsible for generating the Huantraico–Matancilla basalts; MORB-like mantle with low $^{206}Pb/^{204}Pb$, an EM1-type mantle and a mantle component with high $^{207}Pb/^{204}Pb$ and $^{208}Pb/^{204}Pb$ and low Nd isotope ratios that are also dominant in the local main arc.

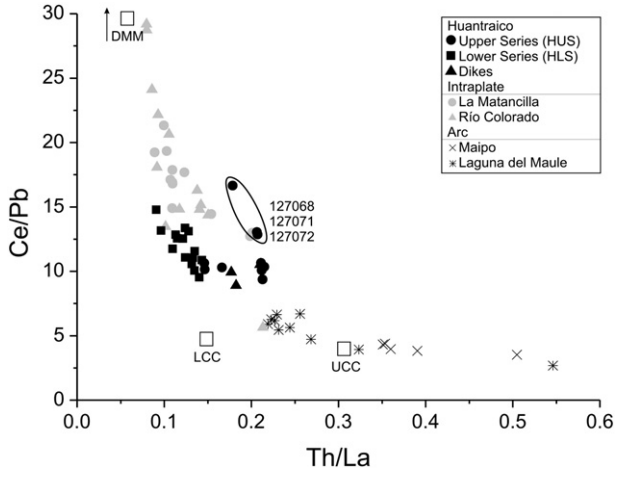

Fig. 9. Trace element ratios show the intermediate character of Huantraico lavas between OIB and arc settings. Also shown are average compositions of Upper and Lower Continental Crust (Gao and Rudnick, 2003) and DMM (Stracke and Bourdon, 2009). Samples 127068, 127071 and 127071 deviate from the main trend towards high Ce/Pb, possibly due to secondary alteration. Note the general increase in Th/La from the Lower to the Upper Huantraico series.

6. Discussion

During the Miocene, characteristic arc-signatures were extended far into the present back-arc area of the Neuquén and Mendoza Provinces (e.g. Kay and Copeland, 2006). Volcanic activity in the Sierra de Huantraico, initiated in the early Miocene, has been suggested to have begun in association with eastward migration of the subducting slab (e.g. Kay et al., 2004) and several contributions deal with the volcanism of the Neuquén and Mendoza provinces (e.g. Bermúdez et al., 1993; Bertotto et al., 2009; Nullo et al., 2002; Saal et al., 1995). Magmatism has been related to mechanical disturbances of the subcontinental mantle as a consequence of subduction beneath the South American continental plate (Skewes and Stern, 1979). By contrast, several explanations for OIB-type back-arc magmatism of the Somuncurá Plateau (northern Patagonia) have been suggested. Kay et al. (1993) refer the OIB-type signature to the presence of hot spots or 'hot fingers' whereas De Ignacio et al. (2001) calls for shallow asthenospheric upwelling caused by slab-rotation and upwelling of a hydrous melt derived from an up-warped mantle transition zone was suggested by Orihashi et al.(2006) and Honda et al. (2006). Stern et al. (1990) divided the Pliocene to Quaternary basalts of the SVZ into two groups; transitional and cratonic, based on trace element content and isotope ratios. The transitional basalts show arc-like geochemical features (acquired either during their generation or in a previous contamination episode) whereas cratonic basalts have a strong OIB-like geochemical signature. La Matancilla basalts are the Miocene counterparts to the cratonic basalts of Stern et al. (1990), showing that such distinct OIB-like geochemical affinities are a long-lived feature of the Andean back-arc. The source of the subduction-related component has been suggested to be the subcontinental lithosphere that has been enriched in Sr, K, Rb, Ba and Th (e.g. Pearce, 1983) by subduction-related fluids. Several authors have shown slab-related metasomatism in the Patagonian mantle (Kilian and Stern, 2002; Kilian et al., 1998; Laurora et al., 2001; Stern, 1989) and a general eastward decrease of slab-components in back-arc samples was recorded by Stern et al. (1990), Gorring and Kay (2001) and Rivalenti et al. (2004). Temporal increases in Th/Nb and Ba/Nb (Fig. 10) and enrichment of LILE (Cs, Rb, Ba and Th) (Fig. 6) in the Sierra de Huantraico lavas, often interpreted as characteristic features of

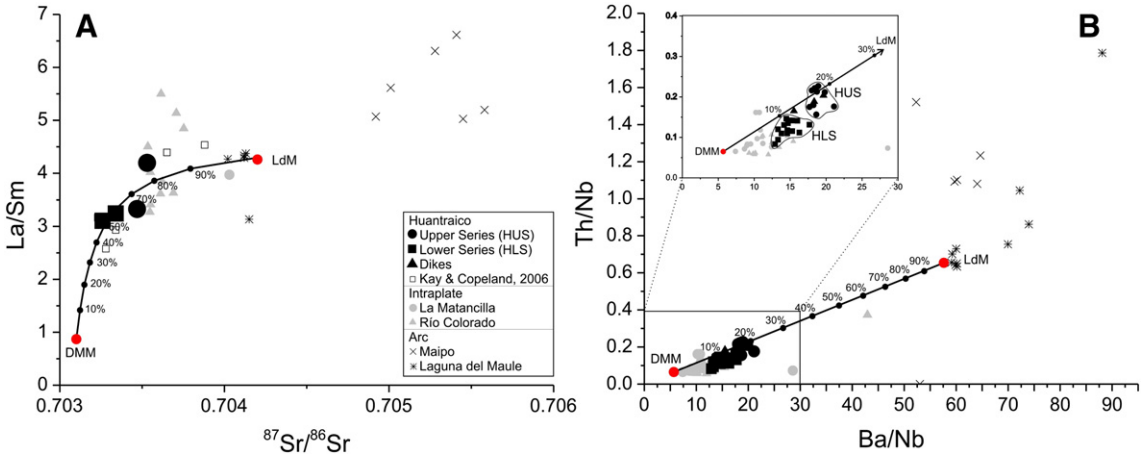

Fig. 10. A) Negative correlation between La/Sm and Sr isotopic ratios in Huantraico lavas and mixing curve between DMM and the arc-like component referred to as LdM (Laguna del Maule). B) Mixing of DMM and a Laguna del Maule component can account for Th/Nb and Ba/Nb in Huantraico magmas.

volcanic arc rocks (Pearce, 1996), may represent an increase of the influence of elements supplied by the Nazca plate. These fluids may be the consequence of eastward migration of the melting window as the result of the shallowing of the subducting slab (Kay and Mancilla, 2001; Kay et al., 2004; Ostera et al., 2000) or they may have been added by a subduction episode prior to the Miocene.

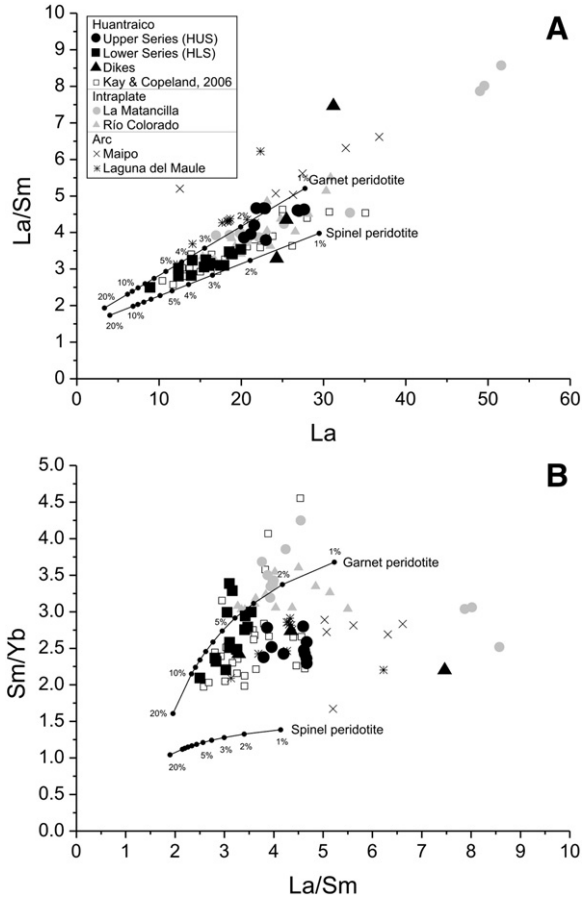

Fig. 11. Batch melting models showing fractional melting of garnet peridotite and spinel peridotite respectively from primitive mantle (Sun & McDonough, 1989). Distribution coefficients are from Rollinson (1993), Fujimaki et al. (1984) and McKenzie and O'Nions (1991).

6.1. Fractional crystallization

There are clear geochemical differences between HLS and HUS and here we investigate whether fractional crystallization models alone can explain these differences. Lavas of the HLS are basalts and lavas of the HUS are slightly more evolved ranging from trachybasalts to trachyandesites. The well correlated variation in the composition of lava flows (Figs. 3, 5, 6) might suggest that the compositional trends have developed through fractional crystallization. Given that the investigated lavas erupted over a time period of several 100 ka, it cannot be assumed that they are directly genetically related. A simple Rayleigh fractionation model has been used to evaluate the hypothesis that the observed major element compositional variation within each of the two groups can be accounted for by extraction of phenocryst phases present in the lavas. Below we consider the evolution by fractional crystallization of magma with composition as the sample with the lowest silica in each group. These lavas contain 5–10 vol.% phenocrysts (mainly olivine and clinopyroxene) and hence do not show evidence of accumulative mafic phases. Possible fractionating minerals are the observed phenocryst phases: olivine, clinopyroxene, plagioclase and minor Fe–Ti-oxides as well as amphibole in the HUS. Decreasing Ni (Fig. 6), increasing SiO_2 and slightly decreasing FeO with decreasing MgO (Fig. 5) with respect to the HLS would require fractionation of olivine. Increasing Al_2O_3/CaO ratios with decreasing MgO (not shown) and fairly good positive correlation between Sr and Ce (not shown), particularly in the Lower Series, indicate a high clinopyroxene/plagioclase ratio of the fractionating phases. A rapid decrease of FeO, a slight decrease of TiO_2 and a decreasing V with a decreasing MgO in HUS suggest that fractionation of Fe–Ti-oxides played a significant role in the more evolved lavas. Relatively small negative Eu anomalies and high constant Sr concentrations (<500 ppm) (Fig. 5) show that plagioclase fractionation was not a dominant factor. Although it was demonstrated that the observed major element composition trends of Huantraico lavas can be reproduced by crystal fractionation, this is not in itself confirmation that fractional crystallization is the only process operating. Trace element ratios reveal that source differences are required to explain some geochemical features, e.g. Th/Nb (HLS = 0.12; HUS = 0.2), La/Sm (HLS = 2.5–3; HUS = 4–4.5), Nb/U (HLS = 20–40; HUS = 12–18), Ba/Ta (HLS = 250; HUS = 300) and Th/Hf (HLS = 0.5–1; HUS = 1–1.3) (see below). We conclude that fractional crystallization played a major role in generating the geochemical evolution within HLS and HUS respectively but that the HUS cannot be related to the HLS simply by crystal fractionation.

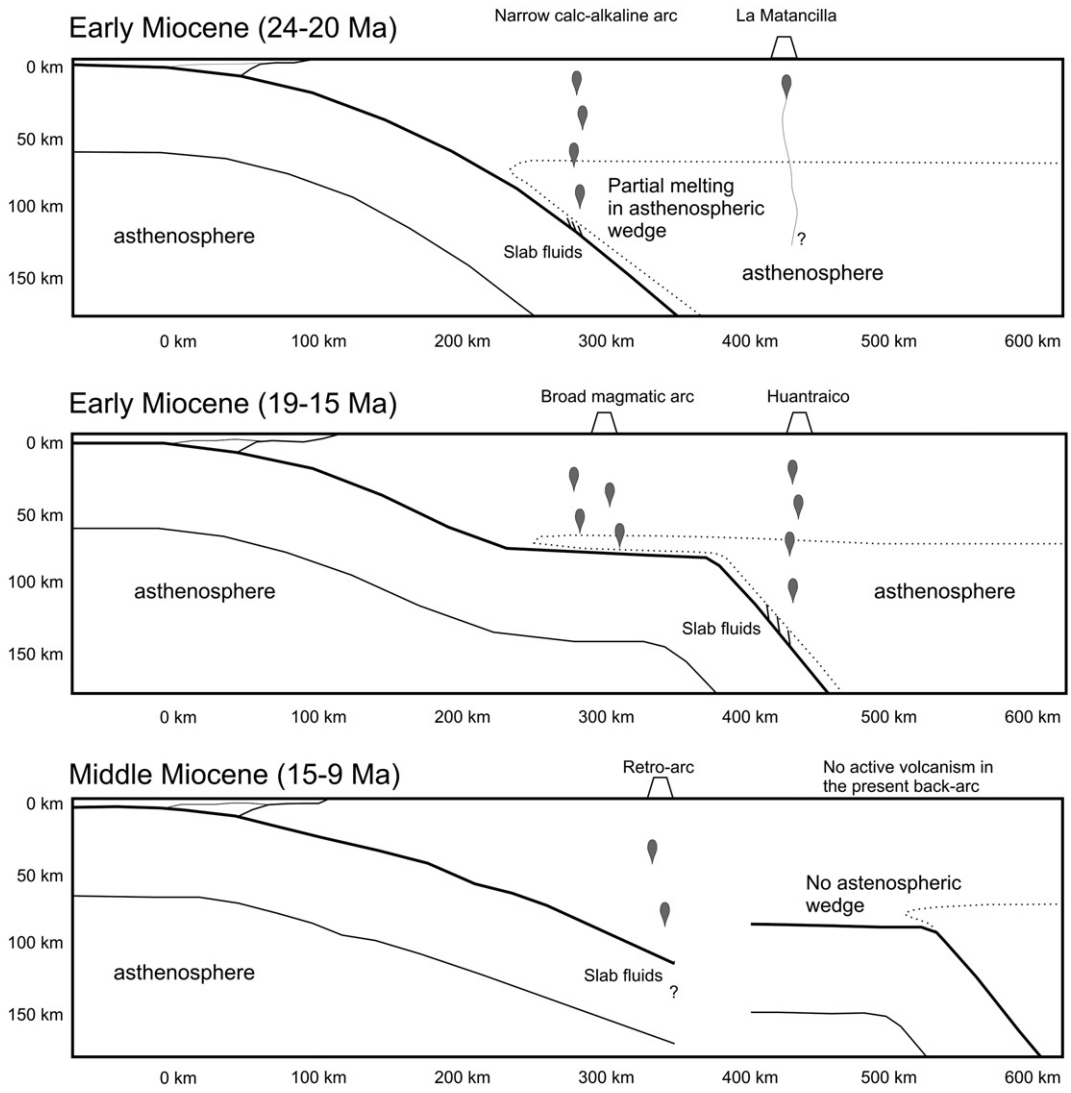

Fig. 12. Cartoon cross section across the Neuquén Basin (near 37°S) for the Miocene illustrating the transition from steep to flat subduction style with impact on magmatic arc. Dotted line denotes the 1300 °C geotherm (Gutscher et al., 2000). Stage 1 (24–20 Ma) show steep subduction (>30° dip) with a narrow calc-alkaline arc ~300 km from the trench and intraplate like volcanic activity occurring in the backarc. Stage 2 sees a transition to early stage flat subduction allowing subduction related fluids to interact with back-arc melts. Partial melting continues in a narrow tongue of asthenospheric material resulting in a broad arc. Stage 3: The subduction zone breaks off leaving a flat slab beneath the Huantraico–Matancilla area. Above the flat part of the slab the asthenospheric tongue is cool and thus no partial melting can occur and volcanism ceases. To the west inclined subduction continued and arc volcanism occurred. The model is based on Gutscher et al. (2000) and Kay and Copeland (2006).

6.2. Crustal assimilation and slab contributions

There are two ways to introduce crustal components; either into the mantle source by sediment subduction and/or fore-arc subduction erosion processes or by contamination of mantle derived magmas within the crust. A likely contaminant might be the deep crustal residue of the widespread Permian–Triassic Choiyoi granite–rhyolite complex, as suggested by Kay and Copeland (2006). Fractionation-independent incompatible trace element ratios such as Th/La (Fig. 9) that are distinguishable between HUS and HLS support a non-genetic relationship between lavas of the two profiles. Assimilation of continental crust might be indicated by high $^{87}Sr/^{86}Sr$ and low $^{143}Nd/^{144}Nd$ isotopic ratios (e.g. Kay and Gordillo, 1994). HUS does show slightly higher $^{87}Sr/^{86}Sr$ compositions than HLS, accompanied by slightly lower $^{143}Nd/^{144}Nd$ ratios (Fig. 8). However, assimilation of typical continental crustal material is unlikely to produce systematic changes as observed in e.g. La/Sm vs. Sr isotopic composition (Fig. 10). Because incompatible trace element concentrations and Sr and Nd isotopic ratios do not relate in a logical way to the type of crust through which the magmas ascended, we conclude that the composition of the Huantraico lavas is determined by processes occurring in the slab and mantle and assimilation of crustal components is not important.

6.3. Degree and depth of melting

Dy/Yb ratios give valuable information to the depth of partial melting. There is a small difference in the HREE ratios between the Lower ($(Dy/Yb)_N = 1.4–1.7$) and the Upper Series ($(Dy/Yb)_N = 1.2–1.4$) indicating that HLS originates from a deeper source than HUS. Relatively flat HREE patterns indicate that garnet was not a significant residual phase during melting inferring that melting occurred at relatively shallow levels for both HLS and HUS.

Simple batch melting models of spinel peridotite and garnet peridotite from a Primitive Mantle source (PM) are shown in Fig. 11. Huantraico magmas are intermediate between these two end members with HUS indicating very low melt fractions (<2%) of spinel peridotite and HLS requiring somewhat higher melt fractions from a slightly deeper source, in accordance with Dy/Yb ratios. Higher melt fractions would be calculated from a model mantle more enriched than PM, and this would physically more readily extract from the source.

6.4. Definitions of contributing source components

At least three different mantle source components are required to explain the trace elemental and isotopic variation in the Huantraico and La Matancilla lavas. There is a continuum of compositions between two end-members in the Huantraico sequence: an arc-like component and a depleted component. The depleted component cannot be the source of La Matancilla lavas and a more OIB-like end-member is invoked. The three components are described below.

6.4.1. The depleted mantle end-member

The depleted end-member dominates in the Lower Huantraico Series and diminishes during the time of emplacement of the Huantraico sequence. The depleted mantle end-member is characterized by low K_2O. Lavas of the Lower Huantraico Series have higher FeO, TiO_2, CaO, Sc, V, Cu, Ni and Cr and lower P_2O_5, Al_2O_3, Rb and Ba, unradiogenic Pb isotopic ratios and low $^{87}Sr/^{86}Sr$ compared to the Upper Series along with relatively low $(La/Sm)_N$ (~2) all pointing towards a depleted mantle source. The correlation between Pb isotope ratios is quite strong and encompasses both our new results and those of Kay and Copeland (2006) (Fig. 9). $^{206}Pb/^{204}Pb$ (18.45–18.6) trend towards arc values although $^{207}Pb/^{204}Pb$ and $^{208}Pb/^{204}Pb$ are lower than observed in arc lavas (Fig. 8) (Holm et al., in preparation). Low K/Nb (200–500), Ce/Nb (2–2.5) and Ba/Nb (<20) is also characteristic of the depleted end-member. The Pb isotopic signature and the low Sr/high Nd isotopic ratios of this end-member are not observed elsewhere in the Mendoza back-arc and we refer to this component as the Huantraico end-member. The Huantraico end-member resembles Depleted MORB Mantle (DMM) (Stracke and Bourdon, 2009) in trace element composition and $^{87}Sr/^{86}Sr$ and Pb isotopic space but requires a less radiogenic $^{143}Nd/^{144}Nd$ ratio.

6.4.2. The Arc-like mantle end-member

The arc end-member is defined to resemble the magmatic source of the local Andean arc (Laguna del Maule lavas are chosen to represent this arc-component). The influence of this component increases from HLS to HUS, e.g. lavas from the Upper Series have $^{87}Sr/^{86}Sr$ ratios of 0.0735, slightly higher than observed in the Lower Series and the Th/Nb ratio is ~0.20 in HUS compared to 0.12 in HLS. The arc-like end-member is also characterized by high LILE/REE, e.g. Ba/La and high Nb/Y, Ce/Y, Ba/Ce, and Ta/La compared to MORB. Arc-like characteristics include high Al_2O_3 (~18 wt.%) and low TiO_2 (<1.8 wt.%) and relatively high Ba/La especially for the Upper Series (>18) as well as low Ta to REE ratios (Fig. 7). A minor increase in Th/La from HLS to HUS also testifies to the increasing addition of an arc-like component (Fig. 9).

6.4.3. The OIB-like end-member

A third component is present in the Early Miocene back-arc mantle, represented by La Matancilla lavas. These have an EM-1 signature and are geochemically similar to the more recent Río Colorado indicating that the OIB-like mantle component has been present in the Andean back-arc over a period of at least 20 Ma. Río Colorado and La Matancilla are characterized by $^{87}Sr/^{86}Sr$ ratios between 0.7035 and 0.704, $^{207}Pb/^{204}Pb$ and $^{208}Pb/^{204}Pb$ similar to Huantraico lavas, but much lower $^{206}Pb/^{204}Pb$ (18.34–18.42) (Fig. 8). La Matancilla lavas have Ba/Nb (~10) and K/Nb (~400) which are higher than in MORB and resembles EM-1 (Zindler and Hart, 1986). An EM-1 type component is also called upon to explain the geochemical variation in the Somuncura plateau (Kay et al., 2007).

6.4.4. Temporal changes in the composition of the Huantraico mantle source

There is a significant time-related change in the Sr–Nd–Pb isotopic ratios of the Huantraico magmas. The range of Sr–Nd–Pb isotopic and key incompatible trace element ratio variation appears to be confined between two end-member compositions; an arc-like end-member and a depleted end-member (described above). The arc-like end-member appears to be similar to the source of Laguna del Maule magmas and its contribution to the Huantraico magmas is constrained by modeling assuming that Laguna del Maule lavas represent 10% melting in the spinel peridotite field (D-values from Stracke and Bourdon, 2009) and that the depleted end-member is similar to DMM with Pb isotopic ratios close to the NHRL. The depleted end-member requires more radiogenic $^{87}Sr/^{86}Sr$ and less radiogenic $^{143}Nd/^{144}Nd$ than Pacific MORB (White et al., 1987) but resembles South Atlantic MORB (Le Roux, 2000). Mixing of these two source end-members adequately explains the isotopic variation (Fig. 8) with HLS requiring a larger proportion of the depleted component than HUS. The temporal change is proposed to be the result of increased slab influence during the emplacement of the Huantraico lavas. Evidence for a similar depleted mantle is not found in more recent rocks in the Neuquén/Mendoza back-arc and seems unique to Huantraico during the Miocene. Two-component mixing is also evidenced by Th/Nb, Ba/Nb and La/Sm (Fig. 10). DMM has low Th/La and high Ce/Pb (0.6 and 34 respectively (Stracke and Bourdon, 2009)) but a few lavas deviate from the main trend defined by mixing between DMM and the arc-component towards high Ce/Pb (Fig. 9) which must be due to processes affecting the magmas subsequent to mantle mixing.

7. Aspects of the Neogene geological evolution in the back-arc

Early Miocene (24–20 Ma) magmatism in the southern Mendoza and northern Neuquén provinces occurred at a time of extension along the entire Andean margin (Jordan et al., 2001; Kay and Copeland, 2006; Muñoz et al., 2000). Magmas with an isotopic signature of enriched OIB type mantle erupted far to the east of the trench (stage 1, Fig. 12). Around this time at Cura Mallín, 26–23 Ma (Jordan et al., 2001), arc magmas (Kay et al., 2006) were erupted. Subsequently 19–17 Ma basaltic to trachyandesitic back-arc lavas with a stronger arc-like signature (e.g. in Huantraico we observe La/Ta = 15–26; Ba/La = 15–32; Ta/Hf = 0.2–4.5 and an isotopic signature of a depleted mantle) with a composition distinctly different than other Neogene Andes magma sources, were erupted in a changing contractional regime (stage 2, Fig. 12). The distinct change at 20 Ma of back-arc lava compositions from La Matancilla to Huantraico magmatism has also previously been noted by several authors (e.g. Kay and Copeland, 2006). During the construction of the Huantraico plateau, volcanic products gradually approach those in subduction zone magmatic rocks by showing an increasing relative depletion in HFSE and higher La/Ta and excess of fluid-mobile elements with the effect of higher Ba/La and lower Nb/U ratios. Amphibole phenocrysts in HUS also testify to a more pronounced hydrous component than in the previously erupted lavas. The temporal development at Huantraico thus may illustrate the incoming of a dehydrating slab below. The arc related magmatism in Huantraico (500 km from the trench) was explained by the development of a flat slab under Payenia by Kay and Copeland (2006). Adding to this hypothesis, we suggest that the change from OIB-type magmatism to arc-type magmatism took place in just a few Ma, from 23 Ma to 18 Ma. The further implication is that the position of the arc and thus the subducting slab moved 150 km eastwards over no more than 5 Ma, a speed of at least 3 cm/a, and a rather dramatic change at around 20 Ma of the plate tectonics may be indicated.

Between 16 and 15 Ma magmatic activity occurred in the Cerro Bayo (Cobbold and Rossello, 2003) and indicated a stationary subduction geometry. Around this latitude arc-type magmatism took place at Charilehue around 15–14 Ma (Spagnuolo et al., 2012) and in Cajon Negro around 16–10 Ma (Jordan et al., 2001) indicating that subduction took place onwards from 16 Ma further west. We infer that for the Huantraico area the eastward advancing flat subduction caused cooling and retreat of the asthenospheric tongue, and thus, after 15 Ma, this or the cessation of relative movement of the lower plate prevented partial

melts from forming above the flat part of the subducting slab (stage 3, Fig. 12). The occurrence of subduction at this time further west may have been caused by a break-off of the flat slab and renewed inclined subduction under the Andes (stage 3, Fig. 12). It is evident that future studies are needed to constrain better the very complex Cenozoic evolution of the South American continental margin, not least along the Southern Volcanic Zone.

8. Conclusions

- The lava succession of the southern Huantraico plateau ranges from basalts to trachyandesites and a single dike cutting the lava sequence has a more evolved composition (trachyte). The ~200 m sequence of lavas display a systematic change with time of incompatible element ratios and Sr, Nd and Pb isotopic compositions.
- Most Huantraico lavas are the result of low degrees of melting in the spinel stability field. There is evidence that Huantraico Lower Series originates from a slightly deeper source and higher melting degrees than Huantraico Upper Series.
- The Huantraico lavas show a temporal increase in the influence of arc-related elements that may indicate that devolatilization in the subduction zone was initiated below Huantraico from just after 20 Ma. The increase in arc influence is likely due to Huantraico Upper Series magma sources having a longer history of metasomatic enrichment by subduction zone components, and the studied Huantraico sequence reflects the dynamic change in source composition over less than 0.5 Ma.
- The increase in subduction input to the magmas is in agreement with an eastward migration of the slab fluid metasomatism in response to a decrease in angle of the subduction in the late Miocene and the end of volcanism in the Huantraico area may indicate the establishment of a flat slab around 15 Ma.
- We invoke a depleted mantle end-member, unique to the Huantraico region, with unradiogenic Pb isotopic compositions, close to the Northern Hemisphere Reference Line, but with Sr and Nd isotope ratios in the range of South Atlantic MORB.
- Mixing of such depleted mantle and an arc-like components explains the Sr–Nd–Pb isotope variation as well as the incompatible trace element variation throughout the Huantraico Series.
- The early Miocene Matancilla lava plateau was emplaced over approximately 4 Ma from the start of the Miocene at 24.4 ± 0.3 (2σ) Ma.
- The Matancilla magmas were derived from an OIB EM-1 type mantle of similar composition to the source of present day backarc magmas of Payenia, and this demonstrates the longevity of this mantle component.

Supplementary data to this article can be found online at http://dx.doi.org/10.1016/j.lithos.2013.08.007.

Acknowledgements

Simon Normann Lauritzen and Jesper Holst are thanked for their assistance during field work. Laurence Page, Toni Larsen and Toby Leeper are thanked for analytical assistance and we thank Jørgen Kystol, GEUS, for excellent major and trace element analyses. Nina Søager is thanked for many fruitful discussions. J. C. Varekamp and an anonymous reviewer contributed with constructive comments to the improvement of the paper. We greatly acknowledge the support to PMH from the Danish Research Council, grant 272-07-0514 and the Faculty of Science for a PhD stipend to CTD.

References

Baker, J., Peate, D., Waight, T., Meyzen, C., 2004. Pb isotopic analysis of standards and samples using a ^{207}Pb–^{204}Pb double spike and thallium to correct for mass bias with a double-focusing MC–ICP–MS. Chemical Geology 211, 275–303.

Bermúdez, A., Delpino, D., 1989. La Provincia basáltica Andesina cuyana (35°–37°S). Asociación Geológica Argentina Revista 44, 28–34.

Bermúdez, A., Delpino, D., Frey, F., Saal, A., 1993. Los basaltos de retroarco extraandinos. In: Ramos, V.A. (Ed.), XII Congreso Geológico Argentino y II Congreso de Exploración de Hidrocarburos, Mendoza, pp. 161–173.

Bertotto, G.W., Cingolani, C.A., Bjerg, E.A., 2009. Geochemical variations in Cenozoic back-arc basalts at the border of La Pampa and Mendoza provinces, Argentina. Journal of South American Earth Sciences 28, 360–373.

Cande, S.C., Kent, D.V., 1992. Revised calibration of the geomagnetic time scale for the Late Cretaceous and Cenozoic. Journal of Geophysical Research 97, 13917–13951.

Cobbold, P.R., Rossello, E.A., 2003. Aptian to Recent compressional deformation, foothills of the Neuquén Basin, Argentina. Marine and Petroleum Geology 20, 429–443.

Dalrymple, G.B., Lanphere, M.A., 1971. $^{40}Ar/^{39}Ar$ technique of K–Ar dating: a comparison with the conventional technique. Earth and Planetary Science Letters 12, 300–308.

De Ignacio, C., López, I., Oyarzún, R., Márquez, A., 2001. The northern Patagonia Somuncura plateau basalts: a product of slab-induced, shallow asthenospheric upwelling? Terra Nova 13, 117–121.

Frey, F.A., Gerlach, D.C., Hickey, R.L., Lopez-Escobar, L., Munizaga-Villavicencio, F., 1984. Petrogenesis of the Laguna del Maule volcanic complex, Chile (36°S). Contributions to Mineralogy and Petrology 88, 133–149.

Fujimaki, H., Tatsumoto, M., Aoki, K., 1984. Partition coefficients of Hf, Zr, and REE between phenocrysts and groundmasses. Journal of Geophysical Research 89, B662–B762.

Gao, S., Rudnick, R.L., 2003. Composition of the continental crust. Treatise on Geochemistry 3 (01), 1–64.

Gonzáles Díaz, E.F., 1979. Descripción geológica de la hoja 31 d, La Matancilla, Carta Geológico-Económica de la República Argentina. Dirección Nacional de Gología y Minería, Boletín no. 173, escala 1:200,000

Gorring, M.L., Kay, S.M., 2001. Mantle processes and sources of Neogene slab window magmas from southern Patagonia, Argentina. Journal of Petrology 42, 1067–1094.

Gudnasson, J., Holm, P.M., Søager, N., Llambías, E.J., 2012. Geochronology of the late Pliocene to recent volcanic activity in the Payenia back-arc volcanic province, Mendoza Argentina. Journal of South American Earth Sciences 37, 191–201.

Gutscher, M.A., Maury, R., Eissen, J.P., Bourdon, E., 2000. Can slab melting be caused by flat subduction? Geology 28, 535–538.

Holm, P.M., Søager, N., Dyhr, C.T., 2013. The role of crust and fluids in the generation of arc magmas in the SVZ of the Andes (in preparation).

Honda, S., Orihashi, Y., Mibe, K., Motoko, A., Sumino, H., Haller, M.J., 2006. Mantle wedge deformation by subducting and rotating slab and its possible implication. Earth, Planets and Space 58, 1087–1092.

Jordan, T.E., Burns, W.M., Veiga, R., Pángaro, F., Copeland, P., Kelley, S., Mpodozis, C., 2001. Extension and basin formation in the Southern Andes caused by increased convergence rate: a mid-Cenozoic trigger for the Andes. Tectonics 20, 308–324.

Kay, S.M., 2001. Tertiary to Recent magmatism and tectonics of the Neuquén Basin between 36°05′ and 38°S latitude. Geólogos Asociados, S.A., Internal report to YPF (Buenos Aires).

Kay, S.M., Copeland, P., 2006. Early to middle Miocene back-arc magmas of the Neuquén Basin: geochemical consequences of slab shallowing and the westward drift of South America. Geological Society of America, Special Paper 407, 185–213.

Kay, S.M., Gordillo, C.E., 1994. Pocho volcanic rocks and the melting of depleted continental lithosphere above a shallowly dipping subduction zone in the central Andes. Contributions to Mineralogy and Petrology 117, 25–44.

Kay, S.M., Mancilla, O., 2001. Neogene shallow subduction segments in the Chilean/Argentine Andes and Andean-type margins. Geological Society of America Abstracts with Programs 34 A-156.

Kay, S.M., Ardolino, A., Franchi, M., Ramos, V., 1993. Origen de la Meseta de Somún Curá: distrbución y geoquímica de sus rocas volcánicas máficas. XII Congreso Geológico Argentino y II Congreso de Exploración de Hidrocarburos, Mendoza, Actas, 4, pp. 236–248.

Kay, S.M., Gorring, M., Ramos, V., 2004. Magmatic sources, setting and causes of Eocene to Recent Patagonian plateau magmatism (36°S to 52°S latitude). Revista de la Asocación Geológica Argentina 59, 556–568.

Kay, S.M., Mancilla, O., Copeland, P., 2006. Evolution of the late Miocene Chachahuén volcanic complex at 37°S over a transient shallow subduction zone under the Neuquén Andes. Evolution of an Andean margin: a tectonic and magmatic view from the Andes to the Neuquén Basin (35°–39° S lat). The Geological Society of America, Special Paper 407, 215–246.

Kay, S.M., Ardolino, A.A., Gorring, M.L., Ramos, V.A., 2007. The Somuncura large igneous province in Patagonia: interaction of a transient mantle thermal anomaly with a subducting slab. Journal of Petrology 48, 43–77.

Kilian, R., Stern, C.R., 2002. Constraints on the interaction between slab melts and the mantle wedge from adakitic glass in peridotite xenoliths. European Journal of Mineralogy 14, 25–36.

Kilian, R., Franzen, C., Koch, M., 1998. The metasomatism of the mantle wedge below the southern Andes: constraints from laser ablation microprobe ICP–MS trace element analysis of clinopyroxenes, orthopyroxenes and fluid inclusions of mantle xenoliths. Terra Nostra 98, 81–82.

Kystol, J., Larsen, L.M., 1999. Analytical procedures in the rock geochemical laboratory of the Geological Survey of Denmark and Greenland. Geology of Greenland Survey Bulletin 184, 59–62.

Laurora, A., Mazzucchelli, M., Rivalenti, G., Vannucci, R., Zanetti, A., Barbieri, M.A., Cingolani, C.A., 2001. Metasomatism and melting in carbonated peridotite xenoliths from the mantle wedge: the Gobernador Gregores case (Southern Patagonia). Journal of Petrology 42, 69–87.

Le Maitre, R.W. (Ed.), 2002. Igneous Rocks. A Classification and Glossary of Terms. Recommendations of the International Union of Geological Sciences Subcommission on the Systematics of Igneous Rocks, 2nd ed., 236 pp. Cambridge.

Le Roux, P.J., 2000. The Geochemistry of Selected Mid-Ocean Ridge Basalts from the Southern Mid-Atlantic Ridge (40–55°S). PhD University of Cape Town.
Litvak, V., Folguera, A., Ramos, V.A., 2008. Determination of an arc-related signature in Late Miocene volcanism over the San Rafael Block, Southern Central Andres (34°30″–37°) Argentina: the Payenia shallow subduction zone. 7th International Symposium on Andean Geodynamics, Niza, pp. 289–291 (Extended Abstracts).
McKenzie, D., O'Nions, R.K., 1991. Partial melt distributions from inversion of rare earth element concentrations. Journal of Petrology 32, 1021–1091.
Muñoz, J., Stern, C.R., Bermúdez, A., Delpino, D., Dobbs, M.F., Frey, F.A., 1989. El volcanismo Plio-Cuarternario a través de los 34°–39°S de los Andes. Asociación Geológica Argentina Revista 44, 270–286.
Muñoz, J., Troncoso, R., Duhart, P., Crignola, P., Farmer, L., Stern, C.R., 2000. The relation of the mid-Tertiary coastal magmatic belt in south-central Chile to the late Oligocene increase in plate convergence rate. Revista Geológica de Chile 27, 177–203.
Nullo, F.E., Stephens, G.C., Otamendi, J., Baldauf, P.E., 2002. El volcanismo del Terciario superior del sur de Mendoza. Revista de la Asociación Geológica Argentina 57, 119–132.
Orihashi, Y., Motoki, A., Haller, M., Sumino, M., 2006. Petrogenesis of Somuncura plateau basalt in an extra-back arc province. Melting of hydrous wadsleyite beneath northern Patagonia. Geochimica et Cosmochimica Acta 70, A463.
Ostera, H.A., Haller, M.J., Linares, E., Joensen, V., 2000. Geochemical evidences and implications on contrasting magma sources at Paramillos Altos Intrusive belt, Southern Mendoza, Argentina. IX Congreso Geológico Chileno, Actas, 1, pp. 669–673.
Ottley, C.J., Pearson, D.G., Irvine, G.J., 2003. A routine procedure for the analysis of REE and trace elements in geological samples by ICP–MS. In: Holland, J.G., Tanner, S.D. (Eds.), Plasma Source Mass Spectrometry: Applications and Emerging Technologies. Royal Society of Chemistry, Cambridge, pp. 221–230.
Pardo-Casas, F., Molnar, P., 1987. Relative motion of the Nazc (Farallon) and South America plates since Late Cretaceous time. Tectonics 6, 233–248.
Pearce, J.A., 1983. The role of sub-continental lithosphere in magma genesis at destructive plate margins. In: Hawkesworth, C.J., Norry, M.J. (Eds.), Continental Basalts and Mantle Xenoliths. Shiva, Nantwich, pp. 230–249.
Pearce, J.A., 1996. A user's guide to basalt discrimination diagrams. In: Wyman, D.A. (Ed.), Trace Element Geochemistry of Volcanic Rocks: Applications for Massive Sulphide Exploration. Geological Association of Canada, Short Course Notes, 12, pp. 79–113.
Perez, M.A., Condat, P., 1996. Geología de La Sierra de Chachahuén. Área CNQ-23: Puelen, Geólogos Asociados, S.A., internal report to YPF, 82 p.
Ramos, V.A., Barbieri, M., 1988. El volcanismo Cenozoico de Huantraico: edad y relaciones isotópicas iniciales, Provincia de Neuquén. Asociación Geológica Argentina Revista 43, 210–223.
Ramos, V.A., Kay, S.M., 2006. Overview over the tectonic evolution of the southern Central Andes of Mendoza and Neuquén (35°–39° S latitude. Evolution of an Andean margin: a tectonic and magmatic view from the Andes to the Neuquén Basin (35°–39° S lat). The Geological Society of America, Special Paper 407, 1–18.
Ramos, V.A., Kay, S.M., 2006. Overview of the tectonic evolution of the southern Central Andes of Mendoza and Neuquén (35°–39°S latitude). Geological Society of America, Special Paper 407, 1–18.
Renne, P.R., Swisher, C.C., Deino, A.L., Karner, D.B., Owens, T.L., DePaolo, D.J., 1998. Intercalibrations of standards, absolute ages and uncertainties in 40Ar/39Ar dating. Chemical Geology 145, 117–152.
Rivalenti, G., Mazzucchelli, M., Laurora, A., Ciuffi, S.I.A., Zanetti, A., Vannucci, R., Cingolani, C.A., 2004. The back-arc mantle lithosphere in Patagonia, South America. Journal of South American Earth Sciences 17, 121–152.
Rollinson, H.R., 1993. Using Geochemical Data. Longman Scientific and Technical, Essex 352.
Saal, A.E., Fery, F.A., Delpino, D., Bermúdez, A., 1995. Temporal geochemical variation in alkalic basalts erupted behind the Andean volcanic front (35°S–37°S): evidence for changing the angle and/or rate of subduction. IUGG XXI General Assembly, Boulder, Colorado (Abstract VA 2, 2A-09).
Skewes, M.A., Stern, C.R., 1979. Petrology and geochemistry of alkali basalts and ultramafic inclusions from the Pali-Aike volcanic field in southern Chile and the origin of the Patagonian plateau lavas. Journal of Volcanology and Geothermal Research 6, 3–25.
Søager, N., Holm, P.M., Llambías, E.J., 2013a. Payenia volcanic province, southern Mendoza, Argentina: OIB mantle upwelling in a backarc environment. Chemical Geology 349–350, 36–53.
Søager, N., Holm, P.M., Llambías, E.J., 2013b. Chemical Geology (in preparation, Submitted for publication).
Somoza, R., 1998. Updated Nazca (Farallón)–South America relative motions during the last 40 my: implications for mountain building in the central Andean region. Journal of South American Earth Sciences 11, 211–215.
Spagnuolo, M.G., Litvak, V., Folguera, A., Bottese, G., Ramos, V.A., 2012. Neogene magmatic expansion and mountain building processes in the southern Central Andes, 36–37°S, Argentina. Journal of Geodynamics 53, 81–94.
Sruoga, P., Rubinstein, N.A., Etcheverría, M.P., Cegarra, M., Kay, S.M., Singer, B., Lee, J., 2008. Estadío inicial del arco volcánic neógeno en la Cordillera Principal de Mendoza (35°S). Reviste de la Asociación Geológica Argentina 63, 454–469.
Stern, C.R., 1989. $^{87}Sr/^{86}Sr$ of mantle xenoliths bearing Plio-Quarternary alkali basalts of the Patagonian Plateau lavas of southernmost South America. Revista de la Asociación Geológica Argentina 44, 402–407.
Stern, C.R., 2004. Active Andean volcanism: its geologic and tectonic setting. Revista Geológica de Chile 31, 161–206.
Stern, C.R., Frey, F.A., Futa, K., Zartman, R.E., Peng, Z., Kyser, K.T., 1990. Trace-element and Sr, Nd, Pb and O isotopic composition of Pliocene and Quaternary alkali basalts of the Patagonian Plateau lavas of southernmost South America. Contributions to Mineralogy and Petrology 104, 294–308.
Stracke, A., Bourdon, B., 2009. The importance of melt extraction for tracing mantle heterogeneity. Geochimica et Cosmochimica Acta 73, 218–238.
Sun, S., McDonough, W.F., 1989. Chemical and isotopic systematics of oceanic basalts: implications for mantle composition and processes. Geological Society of London, Special Publications 42, 313–345.
Thirlwall, M.F., 2000. Inter-laboratory and other errors in Pb isotope analyses investigated using a $^{207}Pb–^{204}Pb$ double spike. Chemical Geology 163, 299–322.
Varekamp, J.C., Hesse, A., Mandeville, C.W., 2010. Back-arc basalts from the Loncopue graben (Province of Neuquen, Argentina). Journal of Volcanology and Geothermal Research 197, 313–328.
Viñes, R.F., 1990. Productive duplex imbrications at the Neuquén Basin thrust belt front, Argentina. In: Letouzey, J. (Ed.), Petroleum and Tectonics in Mobile Belts. Editions Technip, Paris, pp. 69–80.
Vollmer, R., 1976. Rb–Sr and U–Th–Pb systematics of alkaline rocks: the alkaline rocks from Italy. Geochimica et Cosmochimica Acta 40, 283–295.
White, W., Hofmann, A.W., Puchelt, H., 1987. Isotope geochemistry of Pacific Mid-Ocean Ridge Basalt. Journal of Geophysical Research 92, 4881–4893.
Zindler, A., Hart, S., 1986. Chemical Geodynamics. Annual review of Earth and Planetary Sciences 14, 493–571.